Structure and dynamics of the anti-AMCV scFv(F8): effects of selected mutations on the antigen combining site

Caterina Arcangeli [a,*] Cristina Cantale [b] Patrizia Galeffi [b] & Vittorio Rosato [a,c]

[a] *ENEA, Dipartimento FIM, Sezione Calcolo e Modellistica, C.R. Casaccia, Via Anguillarese 301, I-00123 Rome, Italy*

[b] *ENEA, Dipartimento BAS, Sezione Genetica e Genomica Vegetale, C.R. Casaccia, Via Anguillarese 301, I-00123 Rome, Italy*

[c] *Ylichron Srl, c/o ENEA C.R. Casaccia, Via Anguillarese 301, I-00123 Rome, Italy*

Abstract

The recombinant antibody fragment scFv(F8), which recognizes the coat protein of the plant virus AMCV, is characterized by peculiar high *in vitro* stability and functional folding even in reducing environments, making it fit for designing stable antibodies with desired properties. Mutagenesis and functional analysis evidenced two residues, at positions 47 and 58 of the V_H chain, playing a crucial role in the antigen binding recognition.

Here, we used a computational procedure to assess the effects of these mutations on the stability, structure and dynamics of the antigen–binding site. Structural models of the wild type scFv(F8) and of its H47 and H58 mutants were built by homology modelling and assessed by multiple 15.5 ns of molecular dynamics simulations. Computational results indicate that the 47H substitution strongly affects the CDR–H_2 conformation, destabilizes the V_H/V_L interface and confers high conformational flexibility to the antigen–binding site, leading the mutant to functional loss. The mutation at position H58 strenghtens the binding site, bestowing a high antigen specificity on the mutant. The essential dynamics and the analysis of the protein–solvent interface further corroborate the correspondence between the extent of the structurally–determined flexibility of the binding site with the different functional behaviours proved by the wild-type and its mutants. These results may have useful implications for structure–based design of antibody combining site.

Key words: single–chain fragment, molecular dynamics simulation, essential dynamics analysis, structure-function relationship, solvent role

1 Introduction

Single-chain antibody fragments (scFvs), in which the variable heavy (V_H) and light (V_L) chains are connected by an engineered flexible peptide linker, are the most popular format among the recombinant antibodies (Bird et al., 1988; Huston et al., 1988). Such format consistently maintains the binding specificity and affinity of the entire parental antibody IgG, while showing small size and improved properties for diagnostic and therapeutic applications (Presta, 2003; Holliger and Hudson, 2005) and for biotechnology issues (Huston et al., 1988; Harris, 1999). Among the scFvs, the recombinant antibody fragment F8 (scFv(F8)), deriving from a monoclonal antibody raised against the coat protein of the plant virus AMCV (Tavladoraki et al., 1993), has been proved to be expressed as a functional and stable molecule even in reducing environment of both bacteria and plants (Benvenuto et al., 1991; Tavladoraki et al., 1999). This intrinsic stability makes the scFv(F8) a potential candidate molecule for the engineering of stable recombinant antibodies with improved structural and functional properties for practical applications. One of the most common experimental stategy to engineer antibodies is the generation of large collections of antibodies with different specificities followed by a selection based on different properties (e.g. improved stability or specific antigen–binding activity). For these reasons, the scFv(F8) has been used with some success as an intrinsically stable scaffold for antibody phage library generation, and for complementary determining regions (CDR) grafting experiments aimed at antibody "humanizations" for immunotherapy (Desiderio et al., 2001; Donini et al., 2003; Villani et al., 2005, 2008). However, one of the major critical point in engineering customized antibodies is still represented by the lack of the knowledge on the structural and functional role of "each" scFv residue. Due to the time–consuming and cost–expensive experimental approaches, the emerging stategy to the rational design of antibody molecules is based on the synergy between experimental and computational biology. Among the different computational approaches, the combined sequence inspection and protein structural analysis can effectively provide relevant information about the functional role of each antibody residue. The knowledge at atomic level of three–dimensional structure, which is, in turn, the main determinant of the biological function allows to investigate and predict the effects of single amino acids substitution on the antibody properties. An effective use of the scFv(F8) for rational design should, therefore, take advantages from the knowledge of its three–dimensional structure, that is however still lacking.

We have exploited the capabilities of homology modelling to build the three-dimensional structure of the scFv(F8) and of molecular dynamics (MD) simulation to investigate the temporal and structural fluctuations of both protein

* Caterina Arcangeli. E–mail:caterina.arcangeli@casaccia.enea.it

and the surrounding solvent at atomic resolution. In particular, the purpose of the simulations described in this article was to investigate the structural and dynamical changes of the scFv(F8) caused by single amino acid substitutions that were experimentally proved to affect the antigen binding recognition (Galeffi et al., 2004). Indeed, two amino acids at positions 47 (47H) and 58 (58H) of the V_H chain of the scFv(F8) were selected on the basis of sequence inspection and alignment with the crystallized and sequenced antibody databases. In the wild-type scFv(F8), the 47H position is occupied by Leu which is rarely observed in antibody framework being this position normally filled with the large Trp amino acid. This rare substitution was proved to dramatically change the shape of binding pocket of some antibodies (Xu et al., 1999; Trinh et al., 1997; Pellequer et al., 2000) because of its location at the V_H/V_L interface and at the base of the paratope. The relatively conserved Tyr at H58 position (about 50% of murine and human sequences) is replaced by Phe in the V_H chain of the scFv(F8). Such position is part of the CDR–H_2 as defined by Kabat et al. (1991) and therefore is supposed to play a relevant role in the binding recognition. Experimental site-directed mutagenesis and functional analysis, as evaluated by indirect ELISA and immuno-printing experiments (Galeffi et al., 2004), evidenced that replacement of the very rare Leu47H with the almost universal Trp in the scFv(F8) (F8M47 mutant) led to loss of its antigen binding ability; on the contrary the replacement of the Phe58H with the more common Tyr (F8M58) seemed to enhance the efficiency of binding with the antigen (details of experimental methods and ELISA results are given in the Supplementary Data). The double mutant, carrying both the mutations (F8M47M58), appeared to decrease its ability to recognize the antigen (Figure S1 of Supplementary Data).

In order to evaluate these observed differences in functional activity, the changes caused by the selected mutations on the structure and dynamics of the scFv(F8) have been investigated. In addition, because there is no scFv(F8) structure available, to verify the influence of using different homology modelled structures on the MD trajectories and associated dynamical properties, we performed three independent MD simulations of the wild–type scFv(F8) starting from three different homology modelled structures (F8WT, F8WTA and F8WTB). The comparison of the multiple converged trajectories demonstrated that both the dynamics and structural behaviour of the wild–type protein show similarities independently of the starting configuration. The analysis of the trajectories and the application of the essential dynamics to extract the functional concerted motions provide a clear picture of the molecular mechanisms leading to the loss of functionality by the H47 mutant and to the increased antigen activity of the H58 mutant. A strong relationship among the intermolecular contacts, the water–mediated interactions within the binding site and the extent of flexibility has been found. The results also demonstrate that the nature of the residue 47 of the V_H is a determinant for the proper conformation of the CDR–H_2 and the framework scaffold of the V_H/V_L interface. Modifications of the latter significantly alter the general shape of the antigen–

binding site and in turn the functional efficiency. The nature of residue 58 of the V_H affects mainly the shape of the antigen–binding site, endowing the protein with increased affinity for the antigen. Based on these findings and the experimental data, we indicate the structural and dynamical bases of the type of binding exhibited by the wild–type scFv(F8) and its functional mutant. The flexibility observed in the antigen combining site of the wild–type protein suggests an induced–fit binding which evolves to a key–and–lock mechanism in the H58 mutant as supported by the strong stiffness of its antigen–binding site. Although an extensive analysis on a large number of mutants should be required, our results, even though not conclusive, could have implications for the structure–based design aimed at increasing the affinity or specificity toward a specific antigen or at introducing novel functions for practical applications.

2 Methods

2.1 Homology Modelling

The three–dimensional structures used as templates for the construction of homology–derived models of the scFv(F8) were searched in the Brookhaven Protein Data Bank (PDB) (Berman et al., 2002). The templates consisted of three single–chain antibodies which showed sequence homology with the scFv(F8) ranging from 79.1% to 82.6%: the phage library-derived scFv fragment 1F9 from *Mus musculus* (PDB id: 1DZB(A)); the anti-carcinoembryonic antigen scFv fragment MFE-23 from *M. musculus* (1QOK(A)); the scFv fragment of MAB198, raised against human acetylcholine receptor, from *Rattus norvegicus* (1F3R(B)). Further, some isolated V_H and V_L chains of different antibody fragments from *M. musculus* were used as additional templates. In particular, the V_L chains of the Fab fragment of neutralising monoclonal antibody 4C4 (1EJO(L)) and of the engineered anti-CEA scFv diabody from T84.66 scFv (1MOE(A)) were included in the templates for modelling the V_L chain of scFv(F8). The V_H chains of the Fab fragment of 17/9, raised against peptide from influenza virus hemagglutinin (1HIL(B)), the Fab fragment of the monoclonal anti-CD4 antibody Q425 (2ADG(B)) and the Fv fragment of the anti-cytochrome C oxidase antibody 7E2 (1MQK(H)) were used for improving the modelling of the V_H chain of scFv(F8). In these cases, the sequence homology between V_H and V_L chains of scFv(F8) and those of templates was above 90.0% with sequence identity values ranging from 77.6% to 94.7%. The same structural templates were used for all the scFv(F8) mutants. Sequence alignments were derived using CLUSTALW program (Thompson et al., 1994). Structure alignments were obtained and analysed by INSIGHTII v. 98.0 (Biosym/MSI, now Accelrys inc., San Diego, USA) and Protein Structure Comparison Service SSM (http://www.ebi.ac.uk/msd-srv/ssm) (Krissinel and

Henrick, 2004). Both aligned results were inspected and adjusted to minimize the number of gaps and insertions. Homology models of the scFv(F8) structures were generated using MODELLER v6 (Fiser and Sali, 2003). An ensemble of ten models were generated for each target scFv and ranked by their molecular probability density function (pdf) values obtained after highest optimization level. From the ensemble, three different models for the wild–type protein – namely, the best homology–derived model (F8WT), the second (F8WTA) and the last (F8WTB) pdf–ranked models – were selected as starting structures for the MD simulations. For each mutant (F8M47, F8M58, F8M47M58) only the best homology–derived model was chosen as starting structure for the MD simulations. The selection of the best model was made on the basis of the lowest pdf value, the stereochemistry and energy quality as assessed by PROCHECK (Laskowski et al., 1993) and PROSAII (Sippl, 1993). Particular attention was paid to verify the correspondence of the CDR conformations in the models with the common knowledge of their arrangement in other antibodies (Chothia and Lesk, 1987; Morea et al., 1998; Tramontano et al., 1990) (see Results and Discussion section and Supplementary Data).
The multiple alignment figures were generated by using ESPript2.2 (Gouet et al., 1999).

2.2 Molecular Dynamics Simulations

MD simulations were carried out using the GROMACS software package (Spoel et al., 2005) with the OPLS-AA force-field (Jorgensen et al., 1996).
The selected homology–derived models were used as the starting structural coordinates for the simulations.
The protonation state of each protein was modelled for neutral pH, i.e. all lysine residues in the proteins were positively charged and all aspartate and glutamate residues negatively charged. The only histidine residue present in the protein was modelled as neutral with the proton on $N^{\delta 1}$ atom.
Each scFv molecule was placed and centered in a cubic box filled with SCP water molecules (Berendsen et al., 1981) 0.9 nm away from the cell boundary. The number of water molecules (ca. 5900) was slightly different in each case, due to different volumes of cells. To neutralize the total box charge, Cl^- ions were added to each protein system. Ions were added by randomly replacing water molecules. To avoid edge effects and to better describe the condition of full hydration, periodic boundary conditions to each hydrated protein system were applied.
The resulting systems were energy minimized by 50000 steps of steepest-descent minimization, with a tolerance of 50 kJ/mol/nm, then heated and equilibrated. The heating and equilibration protocol here used for the scFv(F8) systems followed that previously applied for the V_H domain of a murine antibody (Voordijk et al., 2000) (details are given in Supplementary Data). After

the 208 ps of initial equilibration, data collection was started with trajectory data saved every 0.2 ps. System temperatures and pressures were coupled separately for protein, solvent and ions to τ_t of 0.1 ps and τ_p of 0.5 ps (Berendsen et al., 1984). The pressure was maintained at 1 bar by the isotropic pressure coupling method. Long-range electrostatic interactions were computed using the particle mesh Ewald (PME) method (Essman et al., 1995). A residue-based cutoff of 0.1 nm was used for the short-range electrostatic and van der Waals interactions. The dielectric constant was set to 1.0. Rotational and translational motions of the system were removed and all bond lengths were constrained with the LINCS algorithm (Hess et al., 1997).
The six MD simulations hereafter indicated by F8WT, F8WTA, F8WTB, F8M47, F8M58 and F8M47M58, consisted of a total run of 15.5 ns.

2.3 Analysis of Trajectories and essential dynamics method

Analyses of the trajectories were performed with tools included in the GROMACS suite and with home–made PERL codes. Structural and dynamical properties were averaged over the last 6.5 ns (i.e. from 9 to 15.5 ns) of system trajectories, unless otherwise noted. The H–bond analysis was performed following the geometric criterion adopted in GROMACS; namely if the donor to acceptor distance was shorter than 0.35 nm and the hydrogen–donor–acceptor angle was lower than 30° an H–bond was assumed to exist during the simulation. We considered as maintaned the intraprotein and water–protein H–bonds which were present in the simulation with a time percentage greater than 60%. Cluster analysis was performed using the Gromos method (Daura et al., 1999). Structure configurations were taken from the MD trajectories at 2 ps intervals. The matrix of atom positional RMSD between pairs of structures was calculated for the C_α atoms of the protein excluding the linker (V_H and V_L chains, namely 1-124 PDB residues and 141-253 residues), the CDR–H_1 (30-35 residues), the CDR–H_2 (50-66 residues), the CDR–H_3 (99-114 residues), the CDR–L_1 (164-178 residues), the CDR–L_2 (194-200 residues) and the CDR–L_3 (233-241 residues). The criterion of similarity for two structures was positional RMSD < 0.10 nm for the C_α atoms of the protein and CDRs.
Essential dynamics method, which provides a quantitative measure of the dynamics, relied on principal component analysis of the covariance matrix of the positional fluctuations of the C_α atoms, as described elsewhere (Amadei et al., 1993). Here each matrix was built from the last 6.5 ns of trajectory, from which overall translational and rotational motions was removed, and its diagonalization yielded the principal directions of the large amplitude concerted motions (essential eigenvectors) that characterize the essential subspace of a protein's internal dynamics. The root mean square inner product (RMSIP) between the essential subspace of different simulated systems was used to assess the convergence of the essential subspace (de Groot et al., 1996). In our analysis

we used the RMSIP value between the first 10 eigenvectors of two different sets, as defined by Amadei et al. (1999). The cosine content of the first eigenvector's projection, an index of the sampling convergence (Hess, 2000), was also calculated.
The electrostatic potentials of the wild–type scFv(F8), the mutants and the coat protein of the AMCV were computed using a continuum electrostatic approach to solve the linearized Poisson–Boltzmann equation by means of APBS program (Baker et al., 2001). The atomic charges and radii of the protein structures were assigned by PDB2PQR program (Dolinsky et al., 2004) using the CHARMM forcefield parameters. In order to simulate the physiological conditions a ionic strength of 150 mM was used. A solvent radius probe of 1.4 $\mathring{A}$ was used to define the dielectric boundary and the ionic exclusion radius was set to 2.0 $\mathring{A}$. The dielectric constants of the proteins and the solvent were kept at 4.0 and 80.0, respectively. For each calculation, the structures were first mapped onto a 3D grid with 97 $\times$ 97 $\times$ 97 points at 1.0 $\mathring{A}$ of spacing resolution and the Debye-Huckel boundary conditions were applied. The resulting rough calculation were used as a boundary condition for focused calculation where the resolution was increased to 0.8 $\mathring{A}$.
The graphic models were made using VMD (Humphrey et al., 1996) and PYMOL (DeLano, W.L. The PyMOL Molecular Graphics System (2002) on World Wide Web http://www.pymol.org).

3 Results and Discussion

In absence of a high resolution crystal structure, we exploited the capability of homology modelling to build structural models of the scFv(F8) and its mutants which were used as starting structural coordinates for the dynamics simulations. Throughout the paper, antibody residues are numbered according to the Kabat nomenclature (Kabat et al., 1991) except for the hypervariable loops (CDRs), which were structure based numbered (Al-Lazikani et al., 1997), unless otherwise noted.

3.1 Homology modelling

Models of the wild–type scFv(F8) and its mutants were constructed by established homology modelling procedures. Antibodies possess a highly conserved framework region (Chothia et al., 1998) and the folds adopted by most of CDR loops are restricted to few main–chain conformations (called canonical structures) (Chothia and Lesk, 1987) for which a large database of potential template crystal structures is now available. For these reasons, molecular models of the immunoglobulin variable region can be built with a reasonably high

level of confidence (Morea et al., 2000; Tramontano, 2006).
In our study, the scFv(F8) was constructed from the 3D coordinates of three scFvs, which showed a sequence homology ranging from 79.1% to 82.6% compared to the scFv(F8). The multiple alignment of the scFv(F8) with the structural template is shown in Figure 1. It is known that the nature of the linker connecting the V_H and V_L chains affects the conformation and flexibility of scFv molecule itself (Raag and Whitlow, 1995) making difficult the prediction of the pairing of the V_H and V_L chains (Stanfield et al., 1993). The three templates here used contain a $(Gly_4Ser)_3$ linker identical to that of the scFv(F8). Thus a proper V_H/V_L orientation should be assured. In addition to the three scFv sequences we also aligned the scFv(F8) sequence with additional isolated V_H and V_L chains derived from different antibody fragments. The resulting multiple alignment evidences additional conserved residues both in the framework and the CDR regions (Figure 2). Indeed, the sequence homology between the additional V_H and V_L templates with those of the scFv(F8) is above 90.0% with sequence identity values ranging from 77.6% to 94.7%. Thus, the use of multiple homologues sequences allowed us to achieve a reliable alignment ensuring a good quality of the homology models. We used the same templates for building all the scFv(F8) mutant models.
The best wild–type and mutant scFv(F8) structures were selected on the basis of different criteria. Beside the general evaluation of structural parameters and the prediction quality, particular attention was paid to the conformation of the CDR loops adopted in the models. All the models obtained for the scFv(F8) wild–type and mutants show the CDR–H_1, CDR–H_2, CDR–L_1, CDR–L_2 and CDR–L_3 folded into the predicted standard canonical structures (Figure S2 and Table S1 of Supplementary Data). A different situation is observed for the CDR–H_3. This loop is highly variable in both sequence and length (Kabat et al., 1991) and its precise modelling remains still difficult. However, several noticeable relationships were found between the sequence and length of the loop and the conformations of CDR–H_3 structures (Morea et al., 1998). The primary sequence of the very long CDR–H_3 loop of scFv(F8) suggested a bulged/torso conformation on the basis of rules stated by Morea et al. (1998). We assume the model as reliable if its CDR–H_3 follows some of these rules. In particular, the models were checked for the presence of the conserved salt-bridge between Arg94 and Asp101 and packing of Arg94 residue against the aromatics at positions 27 and 32 in CDR–H_1 loop. The best models of the mutants and the wild–type protein are shown in Figure 3. All the models shows the same V_H/V_L orientation and similar CDRs conformations (details are given in the Supplementary Data). The quality of the selected models was evaluated by a general analysis of structural and energetic parameters. Results are summarized in Table I, in which the comparison of the Ramachandran plot qualities and goodness factors with those of the templates are reported. The amount of residues belonging to the allowed regions of the Ramachandran plots is higher than 95% for all the scFv(F8) models, indicating reliable homology modelled structures. The interaction energy of each residue with the

remainder of the protein, as calulated by PROSAII (Sippl, 1993) (data not reported) was negative in all the four structures as expected for good models. The best selected scFv(F8) models (F8WT, F8M47, F8M58 and F8M47M58) were used as starting coordinates for MD simulations. Further, in order to verify whether the starting conformation of an MD simulation may significantly affect the results, two additional wild–type scFv(F8) models (F8WTA and F8WTB), whose quality is reported in Table I, were used as starting coordinates for multiple MD simulations.

3.2 Molecular dynamics simulations

Few nanoseconds simulation runs could not be long enough to obtain good thermodynamics averages. However, a number of recent studies reported that simulations within a time range of few nanoseconds were used for extracting reliable conformational and functional features of relatively large proteins (10 ns for about 500 amino acids) (Bianchini et al., 2006; Bocchinfuso et al., 2007) and of antibody systems (1–5 ns for about 250 amino acids) (Voordijk et al., 2000; Nowak, 2004; Krl et al., 2005; Sinha and Smith-Gill, 2005). Thus, we performed 15.5 ns MD simulations of all the scFv(F8) models. The resulting MD trajectories are indicated by F8WT, F8M47, F8M58 and F8M47M58. The simulations replica of the wild–type scFv(F8) were indicated by F8WTA and F8WTB.

3.2.1 Convergence and stability of simulations

As an indicative measure of the stability and conformational drift of the proteins in the simulations, the root mean square deviations (RMSD) of the C_α atoms coordinates from their initial values as a function of simulation time were monitored and reported in Figure 4 (solid line). The RMSD values of the F8WT, F8M47 and F8M58 reach a plateau within 6 ns with small fluctuations around 0.2 nm. A very similar behaviour is observed for both the two replica of the wild–type which undergo stabilization within 6 ns (inset of Figure 4). In contrast, the RMSD time evolution of the F8M47M58 mutant shows an increasing trend. Generally, this behaviour indicates that a protein structure does not reach a stability during the simulation. Similar results were obtained by removing the contribution of the flexible CDR loops from the RMSD analysis (dashed lines in Figure 4).
The cluster analysis described in detail by Daura et al. (1999) is considered an effective tool for judging the convergence of MD simulations (Smith et al., 2002; Brigo et al., 2005) which can be considered achieved when the plot of the number of clusters as a function of time reaches a plateau. Thus, we analysed the number of clusters as a function of cumulative time (every 200 ps) observed

for the entire proteins and for the CDR loops. A maximum number of 29, 30, 23, 32, 20 and 34 clusters for the F8WT, F8WTA, F8WTB, F8M47, F8M58 and F8M47M58 molecules, respectively, were found and their time evolution is shown in Figure 5. The conformational sampling of F8M58 reaches a plateau after 6 ns of simulation. All the three wild–type structures and the F8M47 mutant employ a longer time to steady the number of clusters (approximately 9 ns), whereas the number of clusters observed for the F8M47M58 continues to increase throughout the 15.5 ns trajectory. The exclusion of clusters with only one member structure does not alter significantly these trends (empty circles in Figure 5). The insets of Figure 5 show the number of clusters identified for the flexible CDR loops, that are the regions interested in the antigen–binding recognition. In general, a limited number of conformational states are sampled by the CDRs. The CDR–H_1, CDR–L_2 and CDR–L_3 loops display only one conformation throughout the simulations in all the structures (data not shown). The CDR–H_3 of the F8WT samples a maximum of 14 conformational states and its number of clusters reaches a plateau after 9 ns of simulation, whereas that of CDR–H_2 and CDR–L_1 clearly achieves stable values for the last 6 and 4 ns, respectively. The temporal evolution of the number of clusters observed for the CDR–H_3 and CDR–L_1 loops of the F8M47 mutant reaches stable values within 6 ns, whereas that of the CDR–H_2 shows a long drift of 4 ns followed by a conformational stabilization. A rapid convergence with limited conformational sampling in comparison with the F8WT and F8M47 is observed for all the CDR loops of the H58 mutant. The number of clusters of both the CDR–H_2 and CDR–H_3 loops of the F8M47M58 seems to reach a stable value after 7 ns of simulation. Conversely, the number of clusters identified for the CDR–L_1 loop seems does not converge to stable values. This finding indicates that this loop is still accessing to wide conformational sampling.

The overall results here presented suggest that 15.5 ns of simulation are sufficient to achieve a conformational stability for all the three wild–type structures, the F8M47 and F8M58 mutants. On the contrary, longer simulation times would be required to conclude that all significant conformations were sampled by the F8M47M58. On the basis of these results, the last 6.5 nanoseconds (from 9 to 15.5 ns) of simulation was used to extract the structural and dynamical properties of the F8WT and its replica, as well as of the F8M47 and F8M58 mutants.

The time–averaged (over the last 6.5 ns of simulation) values of the radius of gyration (Rg), total potential and kinetic energies (E_{pot}, E_{kin}) and RMSD of the C_α atoms coordinates from the initial antibody structures are reported in Table II. The Rg, a property linked to the molecule volume and compactness, fluctuates around a mean value of 1.8 nm in all the scFv(F8) structures indicating a structural and globular conservation during the simulations. The mean values of the E_{pot} and E_{kin} are stable during the entire simulations. The RMSD of the C_α atoms coordinates, calculated with respect to the initial structures, indicates an approximative value of 0.22 nm displacement from the initial structures which is a reasonable value for protein molecules. Taking into

account that these simulated systems are homology modelled, we consider our structures to be satisfactory stable and reliable for extracting structural and dynamical features.

3.2.2 Effects of the mutations at position 47H and 58H on the structure and dynamics

The functionality of a macromolecule is strictly related to its dynamical behaviour which is, in turn, strongly affected by the structural architecture. Therefore, we analysed the effects of the single amino acid substitutions on the structural rearrangements and dynamical fluctuations.
The comparison between the representative simulated structures of the mutants and the wild-type protein is shown in Figure 6, where the C_α atom traces of the F8M47 (light gray) and of F8M58 (dark gray) superimposed on those of F8WT (black) are depicted. The overall protein structures are similar although some differences can be observed in specific regions. In particular the conformations of the CDR–H_2, CDR–H_3 and CDR–L_3 loops of the F8M47 mutant significantly differ from those of the wild-type (Figure 6(a)). On the contrary, the structure of the H58 mutant displays remarkably similarity with that of the wild-type, except for the conformation of the CDR–H_3 loop (Figure 6(b)). Interestingly, the initial structures, obtained by homology modelling, did not showed significant differences among them (Figure 3 and Figure S1 of Supplementary Data) suggesting that the structural discrepancies observed after MD simulation are the result of a conformational arrangment in a physiologic solvated environment. The comparison of the superimposition of the three starting wild–type structures with those obtained after MD simulations has evidenced that the converged simulated proteins adopt similar conformation with the exception of the apex of the CDR–H_3 which results to be the most flexible loop (data not shown).
To gain a deeper insight into the structural rearrangements occurring in the mutants, a detailed analysis of the intramolecular hydrogen–bond (H–bond) and salt–bridge networks, were performed and summarized in Table SIV of Supplementary Data and in Table III. Both the interactions are known to play a significant role in stabilizing the antibody structure and modulating the flexibility of the antigen–binding site. The main effect of the Leu47HTrp mutation is the lost of the wild–type 58H–50H H–bond which is replaced by the 47H–50H H–bond (Figure 7(a,b)). In the Phe58HTyr mutant the wild–type 58H–50H H–bond is maintained, and the OH group of the Tyr58 forms an additional H–bond with the 52H residue. (Figure 7(a,c)). Interestingly, such interaction forces the 58H side–chain to point towars the tip of the CDR–H_2 instead of the space normally occupied by the 47H residue as observed in other similar crystallographic structures (PDB id: 1BFV, 1OSP, 2H1P). These apparently small changes generate a cascade of events, leading to fine rearrangements of the CDR loops and of the V_H/V_L interface, which in turn

strongly affects the antigen combining site shape as well as the stability itself of the scFv. In particular, differences are observed in the occurrence of specific H–bonds which are supposed to be crucial for the conformation and stabilization of the CDRs and for the packing of the V_H/V_L interface. The large Arg71H framework residue is considered as determinant for one of the known canonical conformation adopted by the CDR–H_2 loop (Tramontano et al., 1990). As expected on the basis of the rules stated by Tramontano et al. (1990), this residue is hydrogen–bonded to residues belonging to the CDR–H_1 and CDR–H_2 in both the F8WT (Figure 8(a)) (as well as in its replica, Table SIV of Supplementary Data) and H58 (Figure 8(c)) structures. On the contrary, the lack of these interactions in the F8M47 (Figure 8(b)) suggests that the CDR–H_2 loop does not maintain the canonical conformation predicted on the basis of the local sequence (Tramontano et al., 1990) and observed in the starting model structure (Figure S1 and Table SII). This finding seems to be in agreement with the remarked difficulty to reach a conformational convergence as observed in the cluster analysis. The main–chain atoms of the residue 100hH often forms a hydrogen–bond to the OH group of the side–chain of residue 36L (Morea et al., 1998). Such interaction, which is involved in the packing of the V_H/V_L interface, is observed in the F8WT (Figure 8(d)) and F8M58 (Figure 8(f)), but is lacking in the H47 mutant (Figure 8(e)). Again, such interaction is present in both the two replica structures of the wild–type system (Table SIV of Supplementary Data). The lack of this interaction in the F8M47 may confer a high flexibility to its CDR–H_3 loop, which becomes free to move being unconstrained from the rest of the antibody. Further, the interaction between two highly conserved residues at position 38 of the V_L and at position 39 of the V_H which both contain Gln in the scFv(F8) and in more than 90% of the human and murine sequences has been monitored. The H–bond formed between the 38L and 39H residues has been supposed to play a crucial role for maintaining the binding site geometry (Stanfield et al., 1993; Novotn and Haber, 1985; Chatellier et al., 1996), for enhancing the antigen binding affinity (Tan et al., 1998) and for stabilizing the remote part of the V_H/V_L interface (Vargas-Madrazo and Paz-Garca, 2003). Such a "key" interaction is observed in the H58 mutant (Figure 8(i)) while is lacking in both the wild–type (Figure 8(g)) and F8M47 (Figure 8(h)) structures. Changes in the V_H/V_L association can modify the relative position of the CDR loops which, in turn, can alter the general shape of the antigen–binding site, as well as the arrangment of the side–chains that interact with the antigen (Stanfield et al., 1993; Vargas-Madrazo and Paz-Garca, 2003). On these grounds, the results suggest that the H58 mutant has a stable V_H/V_L interface which could confer to it the higher functional performance proved by the experimental data.

The salt–bridge interactions occurring in the wild–type and the F8M47 and F8M58 simulated structures are reported in Table III. The two "key" interactions for the stabilization of V_L chain – the Arg61L–Asp82L (Nowak, 2004) – and the bulged–torso conformation of the CDR–H_3 – the Arg94H–Asp101H salt–bridge (Morea et al., 1998) – are well conserved in all the simulated struc-

tures. On the contrary, the salt–bridges between the Arg96H and Asp101H which provides the wild–type and H58 mutant with further stabilization of the CDR–H_3 loop, is lacking in the F8M47 structure.

The critial role of water molecules in the protein structure and function is well known (Westhof, 1993). Crystallographic studies and calorimetric experiments demonstrated the presence of water molecules at the antigen–binding pocket, where they influence, through H–bond formation, the energy of the interaction with the antigen and help to overcome imperfections in surface complementary shape (Yokota et al., 2003; Kondo et al., 1999; Faelber et al., 2001; Bhat et al., 1994). In this respect, the number and location of bound water molecules in the three structures can be related to their possible antigen binding mechanism. We focused our attention on the hydrogen–bond network made by the protein residues of the antigen combining site of the wild–type scFv(F8) and of its mutant with the surrouding water molecules. Indeed, even if the simulated structures are here antigen free, it is thought that the water molecules can form an invariant structural and functional component at the recognition site (Trinh et al., 1997; Bhat et al., 1994). A number of water molecules structurally bonded to protein residues is identified in all the three structures and depicted in Figure 9. In particular, the putative antigen combining site of both the wild–type and H47 mutant is characterized by an extensive network of ordered solvent molecules. The water network is composed by 10 and 7 molecules for the F8WT (Figure 9(a)) and F8M47 (Figure 9(b)), respectively. In the F8WT these molecules make several hydrogen bonds with protein residues and with other water molecules, forming an intricate three-dimensional network that bridges the V_H and V_L chains (Figure 9(a)). Of particular interest is the water–mediated H–bonding network involving residues of the CDR–L_3 (94L and 96L), CDR–H_2 (62H) and the framework Leu47H residue, in which three water molecules are involved. Other water molecules mediate the interaction between the 45H and the 98L (CDR–L_3) residues and the packing of the 100fH (CDR–H_3) with the 91L (CDR–L_3) and 36L residues. These water molecules seem to play a role in completing the imperfect V_H/V_L interface and therefore in mediating the stabilization of interaction between variable regions. In the F8M47 only one water molecule bridges the V_H (100dH of the CDR—H_3) and V_L (91L of the CDR–L_3) chains as shown in Figure 9(b). The remaining water molecules mediate interactions between residues of the same CDR loop. Namely, the 58H and 62H residues of the CDR–H_2 are water–mediated bound to 50H and Trp47H residues, respectively; the residues 95H and 100gH, which are at the base of the CDR–H_3, are helped to interact by means of a water molecule. A poor water network is observed in the H58 mutant, where only 4 water molecules are present and bound to specific residues of the antigen combining site as shown in Figure 9(c). One water molecule mediates the linking, at the base of the CDR–H_3, between the 96H and 100gH residues. The V_H/V_L interface seems to be tightly packed whithout the help of any water molecule. In addition, it can be inferred from Figure 9(d), which reports the average number of all the

H–bonds formed by the V_H and V_L chains with the solvent molecules, that the H58 mutant makes, on average, less H–bonds with the solvent in comparison to F8WT and F8M47.
The overall results suggest that the mutation at position 58H leads to a compact and well defined antigen combining site in which water molecules are almost excluded, underlying a possible strict shape antigen complementarity in this area. Conversely, a rather large number of solvent molecules are required to fill various cavities, in or surrounding the combinining site of the F8WT and F8M47.
Generally, structural water molecules making strong H–bonds with polar group and the surrounding protein are thought to tighten the protein matrix. However, an interesting computational approach revealed that the binding of buried structural water molecules increase the flexibility of proteins, as reflected by enhanced vibrational entropy (Fischer and Verma, 1999). To determine the flexibility along the sequence and to enlighten differences on the dynamical behaviour of the mutants, the root mean square fluctuations (RMSF) of the C_α atoms were calculated from the last 6.5 ns of the simulations. The RMSF values plotted *versus* the protein residues are reported in Figure 10. The extent of flexibility along the protein sequence of the F8M58 mutant is, on average, slightly lower than that registered for the wild type and H47 mutant. All the structures show the largest values (> 0.25 nm) in correspondence of the solvent–exposed terminal residues, whereas a different distribution of flexibility along the remaining protein sequence is observed. In particular, the F8WT protein shows highly flexible regions (> 0.12 nm) in correspondence of the CDR–H_3, CDR–L_1 loops and of some framework residues of the V_L chain. Similar fluctuation patterns are observed in the F8WTA and F8WTB replica simulated structures (data not shown), suggesting that the starting conformation for the MD simulations does not affect significantly the dynamics of the wild–type. A different pattern of fluctuations is registered in the F8M47, in which all the CDR loops of the V_H chain and the CDR–L_1 show large fluctuations (> 0.12 nm). In addition, several framework residues the V_L chains are also characterized by high values of RMSF. The F8M58 mutant, in which the V_L chain seems to be quite rigid, show low fluctuations in correspondence of some residues of the CDRs of the V_H chain. These differences in the extent of flexibility seems to be also reflected in the number of H–bonds involving the CDR residues observed in the three structures (reported in table SIV of Supplementary Data): the high mobility observed for the CDRs of the wild–type and F8M47, correlates with a few number of H–bonds involving CDR residues, 24 and 20 respectively. On the contrary, the CDR residues of the H58 mutant establish 34 H–bonds, conferring enhanced stiffness to the antigen–binding CDR regions. Computational approches demonstrated that intrinsic fluctuations of the unbound antibody correlate with structural changes induced by the antigen binding (Keskin, 2007). The affinity maturation of hapten–binding antibodies appears to evolve from lower specificity, mediated by induced–fit to higher specificity and reduced plasticity with a more preconfigured binding

site. Antigen–binding antibodies seem to possess preselected locally flexible regions undergoing induced–fit binding and rigid regions providing structural framework (Sinha and Smith-Gill, 2005). These observations point to a functional relevance of the intrinsic flexibility observed in the three scFv(F8) structures. The high values of RMSF observed in the wild–type and F8M47 may correlate with a low stability of antibody–antigen complex, whereas the peculiar stiffness exhibited by the H58 mutant may indicate a key–and–lock binding mechanism characterized by a high antigen specificity.

The analysis of the RMSF is, however, affected by local vibrational motions, which are usually irrelevant for functionality. A powerful tool to filter out small fluctuations from large anharmonic motions, relevant for functionality, is represented by the essential dynamics (ED) method based on the principal component analysis (Amadei et al., 1993; de Groot et al., 1996). The ED analysis performed on the last 6.5 ns of the simulated trajectory was here used to analyse and visualize the overall motions of the three scFv structures. In Table IV the root mean square inner product (RMSIP) between the first 10 eigenvectors in all the simulations is reported. The diagonal values represent the RMSIP between the first 10 eigenvectors extracted from the first and the second half of the trajectory. According to Amadei et al. (1999), the obtained values (> 0.6) show a good convergence of the essential subspace. The reaching of the convergence of the essential subspace of the F8M58 is also confirmed by the low value of cosine content (0.14) of the first principal component, which is a strong indicator of a non–diffusive dynamics (Hess, 2000). The cosine content values obtained for the first eigenvectors of the F8WT, F8WTA, F8WTB (0.31, 0.24 and 0.28) and F8M47 (0.43) seem to indicate that these structures perform a semi–random conformational landscape sampling (Hess, 2000). A pictorial view of the wild–type, H47 and H58 mutants motions along the first eigenvector is shown in Figure 11. The F8WT shows a general collective motion involving all the CDRs of the V_H chain, the CDR–L_1 and a number of residues far from the antigen–binding site (Figure 11(a)). It should be noted that, the extent of motion in correspondence of these regions is low in absolute value (< 0.18) indicating that the protein undergoes restrained movements. As shown in Figure 11(b), large collective motions provided for the CDR–H_1, CDR–H_2, CDR–H_3 and CDR–L_1 are observed for the F8M47 mutant. In particular the apex of the CDR–H_3 seems to collapse into the antigen–binding pocket. The motion along the first eigenvector of the F8M58 is concentrated in the CDR–H_1 and to CDR–H_3, which move concertedly. These results further support the evidence that the wild–type, H47 and H58 mutants show different and peculiar conformational dynamics at the paratope. Such differences, which find a strong correspondence with those obtained by RMSF analysis, may reflect different antigen–binding mechanisms. A computational approach based on normal mode analysis of different proteins including antibodies, demonstrated that unbound conformations have intrinsic tendencies to reconfigure their conformations into the bound one and that the ligand recognition/binding mechanism can be estimated *a priori*, by considering the

assumed conformations under the influence of the collective modes (Keskin, 2007). In this respect, the essential dynamics put into evidence that the main collective motion of the F8M47 mutant is dominated by an extensive bending of the CDR–H_3 down the antigen–binding pocket. Such a motion may hamper the antigen recognition and or binding. This is a likely explanation of the experimental findings.
It has been supposed that the F8 antibody recognizes and binds the coat protein of AMCV in correspondence of a highly conserved site, formed by five aspartic acid residues, that is involved in divalent–cation regulated swelling of the AMCV virus (Tavladoraki et al., 1993). The antibody–antigen binding is supposed to be driven by means of the electrostatic field generated by the molecules and is highly correlated with the electrostatic potential at the surface of the molecules. The electrostatic potentials at solvent–accessible surface of the F8WT and its mutants are shown pictorially in Figure 12. The F8WT and F8M58 mutant show similar electrostatic potentials at the antigen–binding site which is characterized by a positivelly–charged and deep cleft. As expected, both the wild-type and H58 mutant structures (Figure 12(a,c)) have a high degree of complementary in the electrostatic properties of the contacting surfaces with that of the antigen (Figure 12(d)). On the contrary, the F8M47 structure(Figure 12(b)) seems to show a flat antigen-combining site and a low electrostatic complementary with the antigen.

4 Conclusions

In this study, we have analysed the structural and dynamical changes of the scFv(F8) caused by single amino acid susbtitutions that were experimentally proved to affect antigen binding recognition. Given the unvalaibility of three–dimensional structures for the scFv(F8) and its mutants, we have built structural models by homology–modelling and carried out MD simulations. To verify the influence of using different starting models on the MD trajectories and associated dynamical properties we compared multiple trajectories of the wild–type. Such a comparison has evidenced that the starting structure, coming from different homology–derived models, does not significantly affect the conformational space sampled by the wild–type protein, that this system is likely to reach convergence and adopt similar conformation and show alike dynamical properties independently of the starting model structure.
This work has shown that the observed variations in structural and dynamical features of the wild–type and two mutant scFv antibodies correlate with their binding properties experimentally derived. The small number of intramolecular interactions and the large number of structural water molecules at the combining site and at the V_H/V_L interface observed in the wild–type scFv(F8) result in a high conformational flexibility. This flexibility, characterized by few

specific geometrical constraints at the binding site, may allow this antibody to accomodate the antigen through an induced–fit mechanism (Stanfield et al., 1993; Sinha and Smith-Gill, 2005; Sinha et al., 2002). It was suggested that antibody affinity maturation involves a reduction of conformational flexibility though formation of preconfigured binding site specified by intramolecular interactions (Sinha and Smith-Gill, 2005; Keskin, 2007). We observed this structural–driven affinity maturation in the H58 mutant. In particular, the high number of intramolecular H–bonds and salt–bridge interactions observed at the antigen combining site and at the V_H/V_L interface, in which few water molecules are observed, limit the flexibility of the H58 mutant. The stiffness and the highly–defined shape of the antigen site geometry suggest a specific key–and–lock binding mechanism. These observations taken togheter seem to explain the different experimental binding affinities of the wild–type and the functional H58 mutant (Galeffi et al., 2004). Similar results were obtained for monoclonal antibodies which recognize epitopes of hen egg–white lysozyme (Sinha et al., 2002) and for fluorescein–binding antibodies (Thorpe and Brooks, 2007). In these studies, a strict correlation between the large number of intramolecular interactions as well as the decreased protein flexibility and the high–affinity antigen binding was postulated (Sinha et al., 2002; Thorpe and Brooks, 2007). This correspondence further supports the relationship we have found between the structural architecture and dynamical behaviour with the different experimental binding capabilities exhibited by the wild–type and F8M58 mutant. The loss of functionality as experimentally observed in the H47 mutant finds a computational support in the drastic changes occurring at the CDR–H_2 conformation and the V_H/V_L interface. As above stressed, this interface may serve as a pivot for readjustments in the relative position of the two domains and its modification may significantly alter the general shape of the antigen binding site and have functional implications (Chatellier et al., 1996). The structrural changes (few intra–molecular and solvent–protein H–bonds) registered at the V_H/V_L interface reflect an increased flexibility which can produce a lower stability of the antigen–antibody complex. The inspection of the electrostatic potentials at the molecular surface shows that both the wild–type and H58 mutant present a good degree of both geometric surface matching and electrostatic complementary to the antigen at their binding sites. On the contrary, the H47 mutant is lacking of the electrostatic complementary to the antigen. The analysis of the collective motions, which provides insight about the likely binding mechanisms, further corroborates the correspondence between the extent of the structurally–determined flexibility of the binding site with the different functional behaviours proved by the wild-type and its mutants. However, it should be taken into account that the binding mechanism occurring in an anti–protein antibody can follow different structural rules than those observed for the anti–hapten antibodies. In a recently published paper by Acierno et al. (2007), for example, has been postulated that the affinity maturation process of anti–protein antibodies involves the increase of the plasticity and stability of the Fv domain, suggesting

an induced–fit binding rather than a key–and–lock mechanism.
In future computational studies, we will further refine our models by extending the simulation time, and including the antigen structure. The analysis of the structure and dynamics of antibodies in the presence and absence of antigens would be required for a full validation of the binding mechanisms responsible for functional recognition which we have here hypothesized.

Acknowledgments

This work was supported by the FIRB project n. RBNE01W7JB (E–GEN). CA thanks Giulio Gianese and Raffaella Paparcone for help with preliminary technical aspects, Maria Sperandei, Arianna Latini and Marcello Donini for helpful discussions and suggestions.

Appendix

Supplementary Data associated with this article.

References

Acierno, J. P., Braden, B. C., Klinke, S., Goldbaum, F. A., Cauerhff, A., Nov 2007. Affinity maturation increases the stability and plasticity of the fv domain of anti-protein antibodies. J Mol Biol 374 (1), 130–146.
URL http://dx.doi.org/10.1016/j.jmb.2007.09.005

Al-Lazikani, B., Lesk, A. M., Chothia, C., Nov 1997. Standard conformations for the canonical structures of immunoglobulins. J Mol Biol 273 (4), 927–948.
URL http://dx.doi.org/10.1006/jmbi.1997.1354

Amadei, A., Ceruso, M. A., Nola, A. D., Sep 1999. On the convergence of the conformational coordinates basis set obtained by the essential dynamics analysis of proteins' molecular dynamics simulations. Proteins 36 (4), 419–424.

Amadei, A., Linssen, A. B., Berendsen, H. J., Dec 1993. Essential dynamics of proteins. Proteins 17 (4), 412–425.
URL http://dx.doi.org/10.1002/prot.340170408

Baker, N. A., Sept, D., Joseph, S., Holst, M. J., McCammon, J. A., Aug 2001. Electrostatics of nanosystems: application to microtubules and the ribosome. Proc Natl Acad Sci U S A 98 (18), 10037–10041.
URL http://dx.doi.org/10.1073/pnas.181342398

Benvenuto, E., Ords, R. J., Tavazza, R., Ancora, G., Biocca, S., Cattaneo, A., Galeffi, P., Oct 1991. 'phytoantibodies': a general vector for the expression of immunoglobulin domains in transgenic plants. Plant Mol Biol 17 (4), 865–874.

Berendsen, H., Postma, J., van Gunsteren, W., Di Nola, A., Haak, J., 1984. Md with coupling to an external bath. J Chem Phys 81, 3684–3690.

Berendsen, H., Postma, J., van Gunsteren, W., Hermans, J., 1981. Interaction models in relation to protein hydration. In: Pullman, B. (Ed.), Intermolecular forces. D Riedel Publishing Company, Dordrecht, pp. 331–342.

Berman, H. M., Battistuz, T., Bhat, T. N., Bluhm, W. F., Bourne, P. E., Burkhardt, K., Feng, Z., Gilliland, G. L., Iype, L., Jain, S., Fagan, P., Marvin, J., Padilla, D., Ravichandran, V., Schneider, B., Thanki, N., Weissig, H., Westbrook, J. D., Zardecki, C., Jun 2002. The protein data bank. Acta Crystallogr D Biol Crystallogr 58 (Pt 6 No 1), 899–907.

Bhat, T. N., Bentley, G. A., Boulot, G., Greene, M. I., Tello, D., Dall'Acqua, W., Souchon, H., Schwarz, F. P., Mariuzza, R. A., Poljak, R. J., Feb 1994. Bound water molecules and conformational stabilization help mediate an antigen-antibody association. Proc Natl Acad Sci U S A 91 (3), 1089–1093.

Bianchini, G., Bocedi, A., Ascenzi, P., Gavuzzo, E., Mazza, F., Aschi, M., Aug 2006. Molecular dynamics simulation of leishmania major surface metalloprotease gp63 (leishmanolysin). Proteins 64 (2), 385–390.
URL http://dx.doi.org/10.1002/prot.21009

Bird, R., KD, H., JW, J., S, J., BM, K., SM, L., T, L., SH, P., GS, R., Whitlow, M., 1988. Single-chain antigen-binding proteins. Science 242, 423–426.

Bocchinfuso, G., Stella, L., Martinelli, S., Flex, E., Carta, C., Pantaleoni, F., Pispisa, B., Venanzi, M., Tartaglia, M., Palleschi, A., Mar 2007. Structural and functional effects of disease-causing amino acid substitutions affecting residues ala72 and glu76 of the protein tyrosine phosphatase shp-2. Proteins 66 (4), 963–974.
URL http://dx.doi.org/10.1002/prot.21050

Brigo, A., Lee, K. W., Mustata, G. I., Briggs, J. M., May 2005. Comparison of multiple molecular dynamics trajectories calculated for the drug-resistant hiv-1 integrase t66i/m154i catalytic domain. Biophys J 88 (5), 3072–3082.
URL http://dx.doi.org/10.1529/biophysj.104.050286

Chatellier, J., Regenmortel, M. H. V., Vernet, T., Altschuh, D., Nov 1996. Functional mapping of conserved residues located at the vl and vh domain interface of a fab. J Mol Biol 264 (1), 1–6.
URL http://dx.doi.org/10.1006/jmbi.1996.0618

Chothia, C., Gelfand, I., Kister, A., May 1998. Structural determinants in the sequences of immunoglobulin variable domain. J Mol Biol 278 (2), 457–479.
URL http://dx.doi.org/10.1006/jmbi.1998.1653

Chothia, C., Lesk, A. M., Aug 1987. Canonical structures for the hypervariable regions of immunoglobulins. J Mol Biol 196 (4), 901–917.

Daura, X., K, G., B, J., D, S., van Gunsteren WF, AE., M., 1999. Peptide folding: when simulation meets experiment. Angew Chem Int Ed Engl 38, 236–240.

de Groot, B. L., van Aalten, D. M., Amadei, A., Berendsen, H. J., Oct 1996. The consistency of large concerted motions in proteins in molecular dynamics simulations. Biophys J 71 (4), 1707–1713.

Desiderio, A., Franconi, R., Lopez, M., Villani, M. E., Viti, F., Chiaraluce, R., Consalvi, V., Neri, D., Benvenuto, E., Jul 2001. A semi-synthetic repertoire of intrinsically stable antibody fragments derived from a single-framework scaffold. J Mol Biol 310 (3), 603–615.
URL http://dx.doi.org/10.1006/jmbi.2001.4756

Dolinsky, T. J., Nielsen, J. E., McCammon, J. A., Baker, N. A., Jul 2004. Pdb2pqr: an automated pipeline for the setup of poisson-boltzmann electrostatics calculations. Nucleic Acids Res 32 (Web Server issue), W665–W667.
URL http://dx.doi.org/10.1093/nar/gkh381

Donini, M., Morea, V., Desiderio, A., Pashkoulov, D., Villani, M. E., Tramontano, A., Benvenuto, E., Jul 2003. Engineering stable cytoplasmic intrabodies with designed specificity. J Mol Biol 330 (2), 323–332.

Essman, U., Perela, L., Berkowitz, M., Darden, T., Lee, H., Pederson, L., 1995. A smooth particle mesh ewald method. J Chem Phys 103, 8577–8592.

Faelber, K., Kirchhofer, D., Presta, L., Kelley, R. F., Muller, Y. A., Oct 2001. The 1.85 a resolution crystal structures of tissue factor in complex with humanized fab d3h44 and of free humanized fab d3h44: revisiting the solvation of antigen combining sites. J Mol Biol 313 (1), 83–97.
URL http://dx.doi.org/10.1006/jmbi.2001.5036

Fischer, S., Verma, C. S., Aug 1999. Binding of buried structural water in-

creases the flexibility of proteins. Proc Natl Acad Sci U S A 96 (17), 9613–9615.

Fiser, A., Sali, A., 2003. Modeller: generation and refinement of homology-based protein structure models. Methods Enzymol 374, 461–491.
URL http://dx.doi.org/10.1016/S0076-6879(03)74020-8

Galeffi, P., d'Apolito, M., Lombardi, A., Cavicchioni, G., Mancino, T., Sperandei, M., Cantale, C., 2004. A model system to study the structural stability of engineered antibodies: mutants of a scfv specific to amcv. Acta Hort (ISHS) 660, 615–620.

Gouet, P., Courcelle, E., Stuart, D. I., Mtoz, F., Apr 1999. Espript: analysis of multiple sequence alignments in postscript. Bioinformatics 15 (4), 305–308.

Harris, B., Jul 1999. Exploiting antibody-based technologies to manage environmental pollution. Trends Biotechnol 17 (7), 290–296.

Hess, Dec 2000. Similarities between principal components of protein dynamics and random diffusion. Phys Rev E Stat Phys Plasmas Fluids Relat Interdiscip Topics 62 (6 Pt B), 8438–8448.

Hess, B., Bekker, H., Berendsen, H., Fraaije, J., 1997. Lincs: a linear constraint solver for molecular simulations. J Comp Chem 18, 1463–1472.

Holliger, P., Hudson, P., 2005. Engineered antibody fragments and the rise of single domains. Nature Biothecnol 23, 1126–1136.

Humphrey, W., Dalke, A., Schulten, K., Feb 1996. Vmd: visual molecular dynamics. J Mol Graph 14 (1), 33–8, 27–8.

Huston, J. S., Levinson, D., Mudgett-Hunter, M., Tai, M. S., Novotn, J., Margolies, M. N., Ridge, R. J., Bruccoleri, R. E., Haber, E., Crea, R., Aug 1988. Protein engineering of antibody binding sites: recovery of specific activity in an anti-digoxin single-chain fv analogue produced in escherichia coli. Proc Natl Acad Sci U S A 85 (16), 5879–5883.

Jorgensen, W., Maxwell, D., TiradoRives, J., 1996. Development and testing of the opls all-atom force field on conformational energetics and properties of organic liquids. J Am Chem Soc 118, 11225–11236.

Kabat, E., Wu, T., Perry, H., Gottesman, K., Foeller, C., 1991. Sequences of proteins of immunological interest. 5th Ed. NIH Publication No. 91–3242, Bethesda, MD.

Keskin, O., 2007. Binding induced conformational changes of proteins correlate with their intrinsic fluctuations: a case study of antibodies. BMC Struct Biol 7, 31.
URL http://dx.doi.org/10.1186/1472-6807-7-31

Kondo, H., Shiroishi, M., Matsushima, M., Tsumoto, K., Kumagai, I., Sep 1999. Crystal structure of anti-hen egg white lysozyme antibody (hyhel-10) fv-antigen complex. local structural changes in the protein antigen and water-mediated interactions of fv-antigen and light chain-heavy chain interfaces. J Biol Chem 274 (39), 27623–27631.

Krissinel, E., Henrick, K., Dec 2004. Secondary-structure matching (ssm), a new tool for fast protein structure alignment in three dimensions. Acta Crystallogr D Biol Crystallogr 60 (Pt 12 Pt 1), 2256–2268.

URL http://dx.doi.org/10.1107/S0907444904026460

Krl, M., Roterman, I., Piekarska, B., Konieczny, L., Rybarska, J., Stopa, B., Splnik, P., May 2005. Analysis of correlated domain motions in igg light chain reveals possible mechanisms of immunological signal transduction. Proteins 59 (3), 545–554.
URL http://dx.doi.org/10.1002/prot.20434

Laskowski, R., MacArthur, M., Moss, D., Thornton, J., 1993. Procheck: a program to check the stereochemical quality of protein structures. J Appl Cryst 26, 283–291.

Morea, V., Lesk, A. M., Tramontano, A., Mar 2000. Antibody modeling: implications for engineering and design. Methods 20 (3), 267–279.
URL http://dx.doi.org/10.1006/meth.1999.0921

Morea, V., Tramontano, A., Rustici, M., Chothia, C., Lesk, A. M., Jan 1998. Conformations of the third hypervariable region in the vh domain of immunoglobulins. J Mol Biol 275 (2), 269–294.
URL http://dx.doi.org/10.1006/jmbi.1997.1442

Novotn, J., Haber, E., Jul 1985. Structural invariants of antigen binding: comparison of immunoglobulin vl-vh and vl-vl domain dimers. Proc Natl Acad Sci U S A 82 (14), 4592–4596.

Nowak, M., Apr 2004. Immunoglobulin kappa light chain and its amyloidogenic mutants: a molecular dynamics study. Proteins 55 (1), 11–21.
URL http://dx.doi.org/10.1002/prot.10606

Pellequer, J. L., Zhao, B., Kao, H. I., Bell, C. W., Li, K., Li, Q. X., Karu, A. E., Roberts, V. A., Sep 2000. Stabilization of bound polycyclic aromatic hydrocarbons by a pi-cation interaction. J Mol Biol 302 (3), 691–699.
URL http://dx.doi.org/10.1006/jmbi.2000.4033

Presta, L., Aug 2003. Antibody engineering for therapeutics. Curr Opin Struct Biol 13 (4), 519–525.

Raag, R., Whitlow, M., Jan 1995. Single-chain fvs. FASEB J 9 (1), 73–80.

Sinha, N., Mohan, S., Lipschultz, C. A., Smith-Gill, S. J., Dec 2002. Differences in electrostatic properties at antibody-antigen binding sites: implications for specificity and cross-reactivity. Biophys J 83 (6), 2946–2968.

Sinha, N., Smith-Gill, S. J., 2005. Molecular dynamics simulation of a high-affinity antibody-protein complex: the binding site is a mosaic of locally flexible and preorganized rigid regions. Cell Biochem Biophys 43 (2), 253–273.

Sippl, M. J., Dec 1993. Recognition of errors in three-dimensional structures of proteins. Proteins 17 (4), 355–362.
URL http://dx.doi.org/10.1002/prot.340170404

Smith, L. J., Daura, X., van Gunsteren, W. F., Aug 2002. Assessing equilibration and convergence in biomolecular simulations. Proteins 48 (3), 487–496.
URL http://dx.doi.org/10.1002/prot.10144

Spoel, D. V. D., Lindahl, E., Hess, B., Groenhof, G., Mark, A. E., Berendsen, H. J. C., Dec 2005. Gromacs: fast, flexible, and free. J Comput Chem 26 (16), 1701–1718.

URL http://dx.doi.org/10.1002/jcc.20291

Stanfield, R. L., Takimoto-Kamimura, M., Rini, J. M., Profy, A. T., Wilson, I. A., Oct 1993. Major antigen-induced domain rearrangements in an antibody. Structure 1 (2), 83–93.

Tan, P. H., Sandmaier, B. M., Stayton, P. S., Sep 1998. Contributions of a highly conserved vh/vl hydrogen bonding interaction to scfv folding stability and refolding efficiency. Biophys J 75 (3), 1473–1482.

Tavladoraki, P., Benvenuto, E., Trinca, S., Martinis, D. D., Cattaneo, A., Galeffi, P., Dec 1993. Transgenic plants expressing a functional single-chain fv antibody are specifically protected from virus attack. Nature 366 (6454), 469–472.

URL http://dx.doi.org/10.1038/366469a0

Tavladoraki, P., Girotti, A., Donini, M., Arias, F. J., Mancini, C., Morea, V., Chiaraluce, R., Consalvi, V., Benvenuto, E., Jun 1999. A single-chain antibody fragment is functionally expressed in the cytoplasm of both escherichia coli and transgenic plants. Eur J Biochem 262 (2), 617–624.

Thompson, J. D., Higgins, D. G., Gibson, T. J., Nov 1994. Clustal w: improving the sensitivity of progressive multiple sequence alignment through sequence weighting, position-specific gap penalties and weight matrix choice. Nucleic Acids Res 22 (22), 4673–4680.

Thorpe, I. F., Brooks, C. L., May 2007. Molecular evolution of affinity and flexibility in the immune system. Proc Natl Acad Sci U S A 104 (21), 8821–8826.

URL http://dx.doi.org/10.1073/pnas.0610064104

Tramontano, A., May 2006. The role of molecular modelling in biomedical research. FEBS Lett 580 (12), 2928–2934.

URL http://dx.doi.org/10.1016/j.febslet.2006.04.011

Tramontano, A., Chothia, C., Lesk, A. M., Sep 1990. Framework residue 71 is a major determinant of the position and conformation of the second hypervariable region in the vh domains of immunoglobulins. J Mol Biol 215 (1), 175–182.

Trinh, C. H., Hemmington, S. D., Verhoeyen, M. E., Phillips, S. E., Jul 1997. Antibody fragment fv4155 bound to two closely related steroid hormones: the structural basis of fine specificity. Structure 5 (7), 937–948.

Vargas-Madrazo, E., Paz-Garca, E., 2003. An improved model of association for vh-vl immunoglobulin domains: asymmetries between vh and vl in the packing of some interface residues. J Mol Recognit 16 (3), 113–120.

URL http://dx.doi.org/10.1002/jmr.613

Villani, M. E., Morea, V., Consalvi, V., Chiaraluce, R., Desiderio, A., Benvenuto, E., Donini, M., May 2008. Humanization of a highly stable single-chain antibody by structure-based antigen-binding site grafting. Mol Immunol 45 (9), 2474–2485.

URL http://dx.doi.org/10.1016/j.molimm.2008.01.016

Villani, M. E., Roggero, P., Bitti, O., Benvenuto, E., Franconi, R., Jun 2005. Immunomodulation of cucumber mosaic virus infection by intrabodies se-

lected in vitro from a stable single-framework phage display library. Plant Mol Biol 58 (3), 305–316.
URL http://dx.doi.org/10.1007/s11103-005-4091-0

Voordijk, S., Hansson, T., Hilvert, D., van Gunsteren, W. F., Jul 2000. Molecular dynamics simulations highlight mobile regions in proteins: A novel suggestion for converting a murine v(h) domain into a more tractable species. J Mol Biol 300 (4), 963–973.
URL http://dx.doi.org/10.1006/jmbi.2000.3890

Westhof, E., 1993. Water and biological macromolecules. Boca Raton: CRC Press.

Xu, J., Deng, Q., Chen, J., Houk, K. N., Bartek, J., Hilvert, D., Wilson, I. A., Dec 1999. Evolution of shape complementarity and catalytic efficiency from a primordial antibody template. Science 286 (5448), 2345–2348.

Yokota, A., Tsumoto, K., Shiroishi, M., Kondo, H., Kumagai, I., Feb 2003. The role of hydrogen bonding via interfacial water molecules in antigen-antibody complexation. the hyhel-10-hel interaction. J Biol Chem 278 (7), 5410–5418.
URL http://dx.doi.org/10.1074/jbc.M210182200

Figure Legends

Figure 1
Multiple sequence alignment of the wild–type scFv(F8) with the structural scFvs templates 1DZB(A), 1F3R(B) and 1QOK(A). The unsolved residues of the $(Gly_4Ser)_3$ linker in the 1DZB(A) and 1QOK(A) crystal templates are not reported and are replaced with dots. The remainder dots represent deletions. Strictly conserved residues have a black background. Well conserved residues are shown in black boldface. Conserved residues in at least half of sequences are boxed. Numbers above sequences represent residue numbering of the 1DZB(A).

Figure 2
(a) Multiple sequence alignment of the V_H chain of the F8WT with those derived from the structural templates 2ADG(B), 1HIL(B) and 1MQK(H). The secondary structures and sequence numbers are assigned according to 2ADG(B), which shows the highest sequence identity (81.6%) with F8WT.
(b) Multiple sequence alignment of the V_L chain of the F8WT with those derived from the structural templates 1EJO(L) and 1MOE(A). The secondary structures and sequence numbers are assigned according to 1EJO(L), which shows the highest sequence identity (94.7%) with F8WT.
Numbers below sequences represent residue numbering according to the Kabat nomenclature of the F8WT. Strictly conserved residues have a black background. Well conserved residues are shown in black boldface. Conserved residues in at least half of sequences are boxed.

Figure 3
Ribbon representation of (a) F8WT, (b) F8M47, (c) F8M58 and (d) F8M47M58 model structures. CDR–H_1, *pink*; CDR–H_2, *mauve*; CDR–H_3, *purple*; CDR–L_1, *cyan*; CDR–L_2, *iceblue*; CDR–L_3, *blue*; 47H and 58H residues (ball and stick), *green*.

Figure 4
C_α RMSD of the whole proteins (solid line) and of the proteins after removing the contribution of the CDR loops (dashed line) with respect to the equilibrated conformations as a function of simulation time. Inset: C_α RMSD of the F8WTA (dashed line) and F8WTB (dotted line) proteins with respect to the equilibrated conformations as a function of simulation time.

Figure 5
Number of total protein clusters (solid circles) and number of protein clusters with more than one member structures (empty circles, squares and diamonds) as a function of simulation time. Inset: Number of clusters with more than one member structures for the CDR–H_2 (squares), CDR–H_3 (diamonds) and

CDR–L_1 (circles) loops.

Figure 6
((a) Superposition of the C_α atoms of F8M47 (light gray) onto those of wild–type scFv(F8) (black). (b) Superposition of the C_α atoms of F8M58 (dark gray) onto those of wild–type scFv(F8) (black). The CDR–H_2, CDR–H_3 and CDR–L_1 loops are labelled. The 47H and 58H residues are shown. For a better comparison, the V_H and V_L chains are depicted as separate C_α traces and their relative actual orientation is not respected.

Figure 7
H–bonding network of the 47H and 58H residues in the F8WT (a), F8M47 (b) and F8M58 (c) simulated structures. Protein diagrams are from representative snapshots of the last 6.5 ns of the simulations. Hydogend–bonds are depicted as dashed lines and the 47H and 58H residues are also labelled.

Figure 8
Comparison of selected H–bonds of the scFv(F8) wild–type and its mutants. Left panel, H–bonding network of Arg71H with residues of CDR–H_1 and CDR–H_2: F8WT, (a), F8M47, (b) and F8M58, (c). Middle panel, H–bond between 100hH residue belonging to CDR–H_3 with residue 36 of V_L chain: F8WT, (d), F8M47, (e) and F8M58, (f). Right panel, H–bond of residue 39 of V_H chain with residue 38 of V_L chain: F8WT, (g), F8M47, (h) and F8M58, (i). Protein diagrams are from representative snapshots of the last 6.5 ns of the simulations. Hydogend–bonds are depicted as dashed lines. Residues and loops are labelled.

Figure 9
Hydrogen bonding network of water molecules at the antigen–binding pocket and at V_H/V_L interface of the wild-type (a), H47 (b) and H58 (c) mutants. The hydrogen bonds are depicted as dashed lines. Residues involved in hydrogen–bonds with solvent are labelled. V_H chain, *pink*; V_L chain, *iceblue*; CDR–H_2 residues, *mauve*; CDR–H_3 residues, *purple*; CDR–L_1 residues, *cyan*; CDR–L_3 residues, *blue*; 47H and 58H residues, *green*. Protein diagrams are from representative snapshots of the last 6.5 ns of simulation. (d) Average number of all H–bonds formed between solvent molecules and residues of V_H (circle) and of V_L (square) chains.

Figure 10
RMSF values of C_α atoms calculated from equilibrated trajectory (9-15.5 ns) as a function of residue number. The residue are numbered as they appear in the PDB file. The peaks above the horizontal line, which represents the average value, correspond to the flexible residues. The horizontal elements indicate the CDR loops for the V_H (black bars) and V_L (grey bars) chains.

Figure 11
Twenty-five configurations obtained by considering the C_α motions due to the first eigenvector for F8WT (a), F8M47 (b) and F8M58 (c). The colouring scheme shows the relative extent of motion, from low (blue) to high (red) mobility. The maximum and minimum values of the eigenvector are indicated. The CDR loops showing concerted motions are labelled.

Figure 12
Electrostatic surface potential of F8WT (a), F8M47 (b), F8M58 (c) and coat protein of AMCV (d), as calculated by APBS program. The view is along the antigen combining site. The CDR loops of the scFvs are labelled and the 47H (green) and 58H (magenta) residues are depicted as sticks. The structure of the AMCV trimer (asymmetric unit) has been homology derived from the TBSV, a virus with a known similar structure (PDB id: 2TBV). The three putative binding sites formed by the aspartic residues (green, sticks) are evidenced by dotted circles. Red and blue colors indicate potential values going from -10 kT/e to +10 kT/e (a-c) and from -15 kT/e to +15 kT/e (d).

Table I – Quality parameters of templates and model structures

Structure	pdf value[a]	G–factor[b]	Ramachandran plot quality (%)[c]		
			allowed	general	disallowed
1DZB(A)[d]		-0.65	97.4	2.1	0.5
1F3R(B)		-0.72	98.1	0.0	1.9
1QOK(A)		0.19	99.5	0.0	0.5
1EJO(L)		0.25	95.9	0.0	1.1
1MOE(A)		0.13	97.0	1.5	1.5
1HIL(B)		-0.17	99.5	0.6	0.0
2ADG(B)		0.20	98.9	1.1	0.0
1MQK(H)		0.96	98.1	0.9	0.9
F8WT[e]	14782.0576	-0.18	97.1	1.4	1.4
F8M47	14955.6113	-0.20	95.7	1.9	2.4
F8M58	14894.1377	-0.22	98.1	0.5	1.4
F8M47M58	14729.8838	-0.17	95.2	2.4	1.4
F8WTA[f]	15010.1523	-0.29	97.1	1.0	1.9
F8WTB	15416.6328	-0.25	97.1	0.0	2.9

[a] The values of the molecular probability density function (pdf) of the different scFv(F8) models are created by MODELLER.
[b] Goodness factor (G-factor) shows the quality of overall bond and angle distances. The score should be above -0.50 for a reliable model.
[c] Ramachandran plot qualities shows the amount of residues belonging to the allowed, general and disallowed region of the plot. A good quality model would be expected to have over 90% in the allowed regions.
[d] The PDB codes; in parenthesis is indicated the chain of the crystal templates used for homology modelling.
[e] The best homology-modelled structures.
[f] The two additional homology-modelled structures of the wild–type scFv(F8).

Table II – Selected properties of the three wild–type scFv(F8) structures and of the mutants calculated from the last 6.5 ns of MD simulated energies and trajectories

Structures	R_g (nm)[a]	C_α RMSD (nm)[b]	E_{pot} (10^5 KJ/mol)[c]	E_{kin} (10^4 KJ/mol)[d]
F8WT	1.81 ± 0.009	0.24 ± 0.014	-2.96 ± 0.038	5.37 ± 0.026
F8WTA	1.82 ± 0.012	0.23 ± 0.015	-2.97 ± 0.038	5.37 ± 0.026
F8WTB	1.82 ± 0.013	0.24 ± 0.016	-2.96 ± 0.039	5.37 ± 0.026
F8M47	1.80 ± 0.010	0.22 ± 0.011	-2.97 ± 0.038	5.37 ± 0.026
F8M58	1.80 ± 0.008	0.20 ± 0.015	-2.96 ± 0.038	5.37 ± 0.026

[a] R_g, radius of gyration.
[b] C_α RMSD, root mean square deviations of C_α atoms of the proteins.
[c] E_{pot}, potential energy.
[d] E_{kin}, kinetic energy.

Table III – Listing of salt–bridges present in the three wild–type scFv(F8) structures and mutants during the last 6.5 ns of simulations

Salt–bridge[a]	Regions[b]	Wild–type[c]	F8M47	F8M58
ARG 38 V_H – GLU 46 V_H	FR–FR	Υ Υ Υ [d]	Υ	Υ
ARG 38 V_H – ASP 86 V_H	FR–FR	Υ Υ Υ	Υ	-
ARG 44 V_H – ASP 42 V_H	FR–FR	- - -	-	Υ
ARG 44 V_H – GLU 46 V_H	FR–FR	Υ Υ Υ	Υ	Υ
ARG 66 V_H – ASP 86 V_H	FR–FR	Υ Υ Υ	Υ	Υ
ARG 94 V_H – ASP 101 V_H	FR–H_3	Υ Υ Υ	Υ	Υ
ARG 96 V_H – ASP 101 V_H	H_3–H_3	Υ Υ Υ	-	Υ
ARG 24 V_L – ASP 70 V_L	L_1–FR	Υ Υ Υ	Υ	Υ
LYS 39 V_L – ASP 81 V_L	FR–FR	Υ Υ Υ	Υ	Υ
ARG 61 V_L – ASP 81 V_L	FR–FR	Υ Υ Υ	Υ	Υ
ARG 61 V_L – ASP 82 V_L	FR–FR	Υ Υ Υ	Υ	Υ
ARG 68 V_L – ASP 30 V_L	FR–L_1	Υ Υ Υ	Υ	Υ
LYS 103 V_L – GLU 105 V_L	FR–FR	Υ Υ Υ	Υ	Υ
ARG 108 V_L – GLU 105 V_L	FR–FR	- - -	Υ	-
ARG 44 V_H – ASP 1 V_L	FR–FR	Υ - Υ	Υ	-
ARG 96 V_H – GLU 55 V_L	H_3–L_2	Υ Υ -	Υ	-

[a] The salt–bridge formation is inferred if the distance between a side–chain oxygen of Asp or Glu and a side–chain nitrogen of Arg, Lys or His is within 0.4 nm.

[b] Antibody regions: FR, framework residue; L_{1-3} complementary determining regions of the V_L chain; H_{1-3} complementary determining regions of the V_H chain.

[c] The three columns refer to F8WT, F8WTA and F8WTB.

[d] Υ, salt–bridge present during the simulation.

Table IV – RMSIP between the first ten eigenvectors in the three wild–type replica and two mutant simulations

	F8WT	F8WTA	F8WTB	F8M47	F8M58
F8WT	0.76[a]	0.68	0.60	0.68	0.68
F8WTA		0.68	0.60	0.63	0.66
F8WTB			0.68	0.66	0.65
F8M47				0.73	0.65
F8M58					0.75

[a] The diagonal values represent the RMSIP beetween the first 10 eigenvectors extracted from the first and the second half of the trajectory.

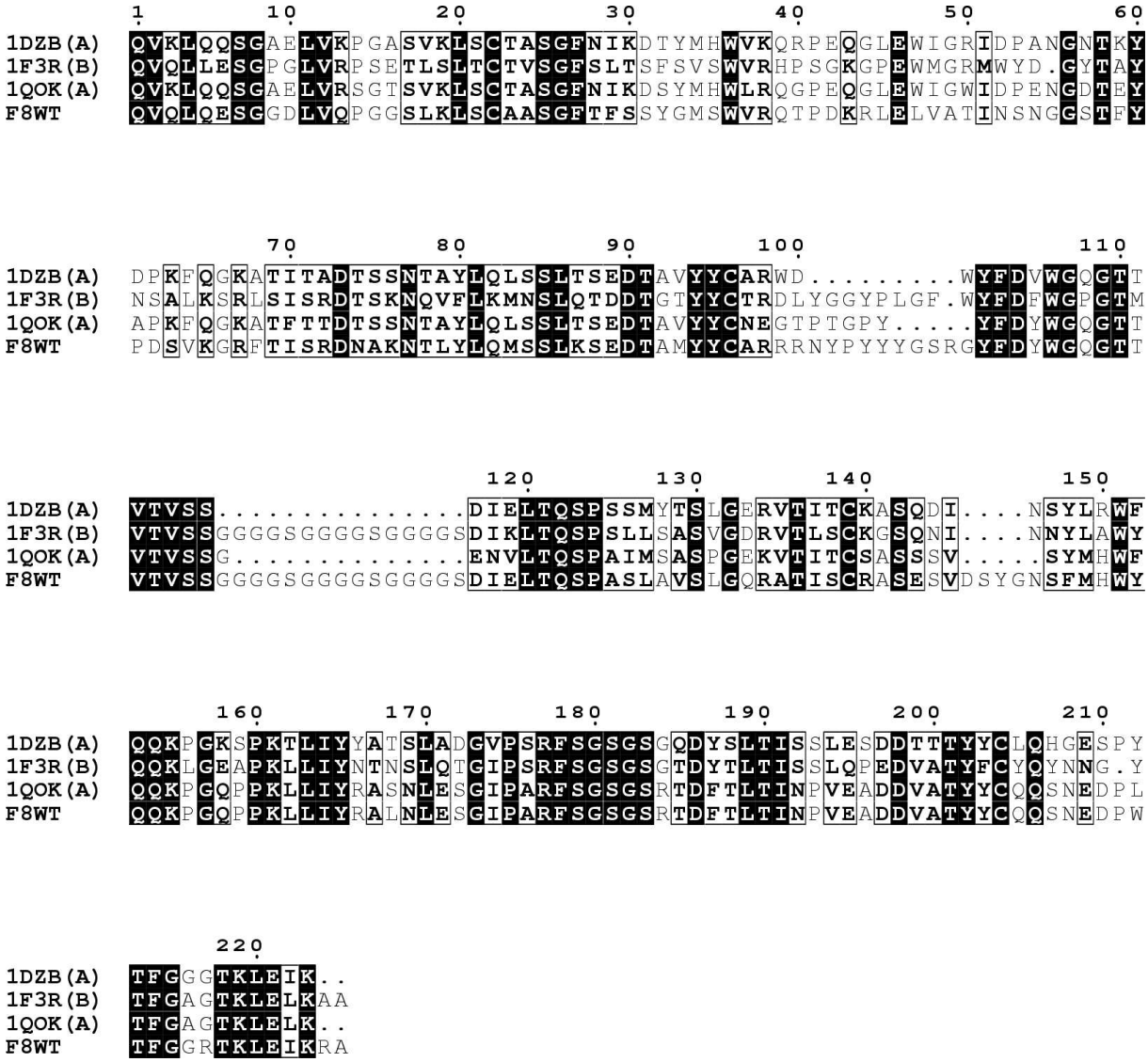

Fig. 1.

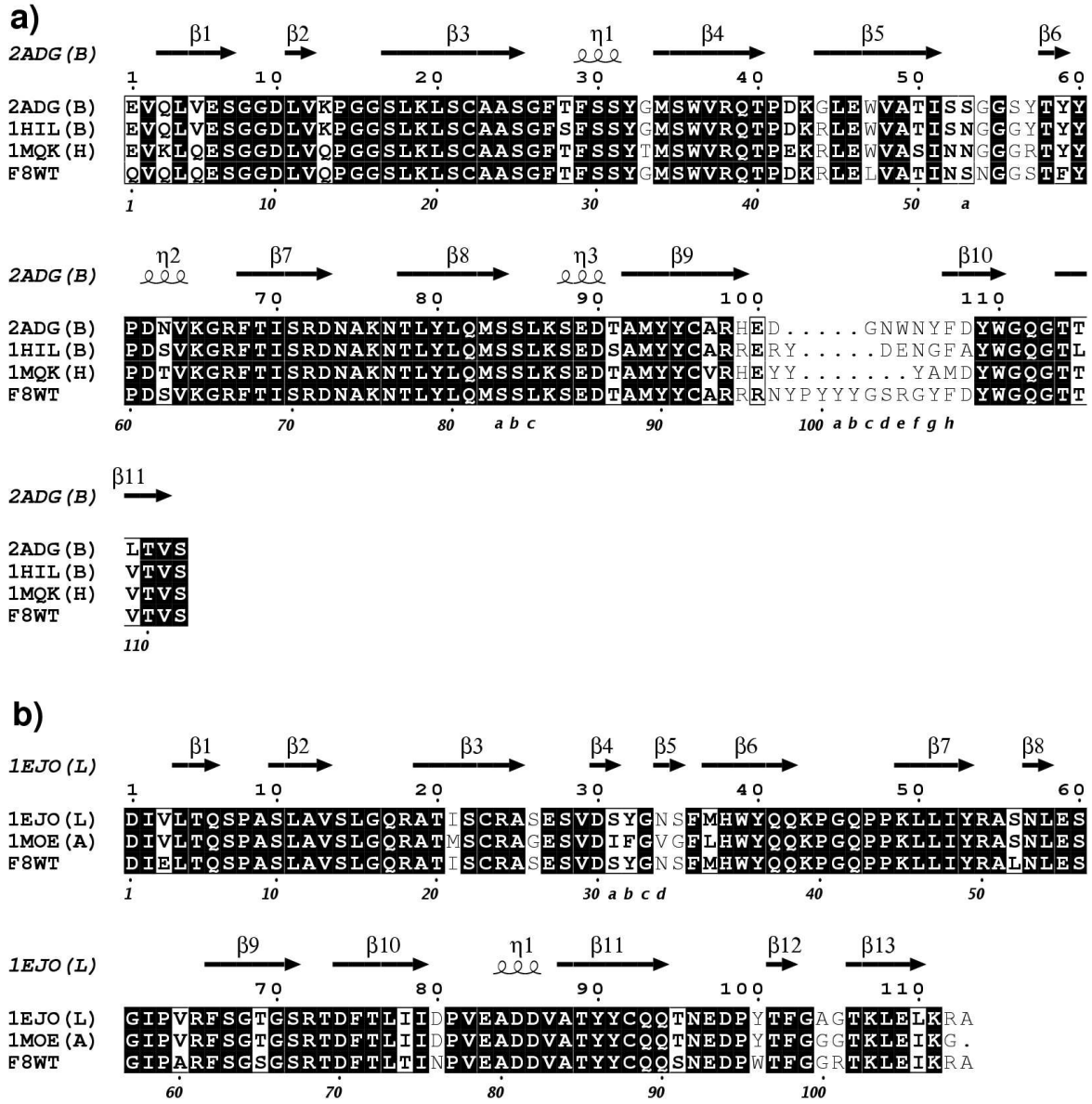
a)
2ADG (B)
β1 β2 β3 η1 β4 β5 β6
2ADG (B) EVQLVESGGDLVKPGGSLKLSCAASGFTFSSYGMSWVRQTPDKGLEWVATISSGGSYTYY
1HIL (B) EVQLVESGGDLVKPGGSLKLSCAASGFSFSSYGMSWVRQTPDKRLEWVATISNGGGYTYY
1MQK (H) EVKLQESGGDLVQPGGSLKLSCAASGFTFSSYTMSWVRQTPEKRLEWVASINNGGGRTYY
F8WT QVQLQESGGDLVQPGGSLKLSCAASGFTFSSYGMSWVRQTPDKRLELVATINSNGGSTFY
η2 β7 β8 η3 β9 β10
2ADG (B) PDNVKGRFTISRDNAKNTLYLQMSSLKSEDTAMYYCARHED.....GNWNYFDYWGQGTT
1HIL (B) PDSVKGRFTISRDNAKNTLYLQMSSLKSEDSAMYYCARREKY.....DENGFAYWGQGTL
1MQK (H) PDTVKGRFTISRDNAKNTLYLQMSSLKSEDTAMYYCVRHEYY.....YAMDYWGQGTT
F8WT PDSVKGRFTISRDNAKNTLYLQMSSLKSEDTAMYYCARRRNYPYYYGSRGYFDYWGQGTT
β11
2ADG (B) LTVS
1HIL (B) VTVS
1MQK (H) VTVS
F8WT VTVS
b)
1EJO (L)
β1 β2 β3 β4 β5 β6 β7 β8
1EJO (L) DIVLTQSPASLAVSLGQRATISCRASESVDSYGNSFMHWYQQKPGQPPKLLIYRASNLES
1MOE (A) DIVLTQSPASLAVSLGQRATMSCRAGESVDIFGVGFLHWYQQKPGQPPKLLIYRASNLES
F8WT DIELTQSPASLAVSLGQRATISCRASESVDSYGNSFMHWYQQKPGQPPKLLIYRALNLES
β9 β10 η1 β11 β12 β13
1EJO (L) GIPVRFSGTGSRTDFTLIIDPVEADDVATYYCQQTNEDPYTFGAGTKLELKRA
1MOE (A) GIPVRFSGTGSRTDFTLIIDPVEADDVATYYCQQTNEDPYTFGGGTKLEIKG.
F8WT GIPARFSGSGSRTDFTLTINPVEADDVATYYCQQSNEDPWTFGGRTKLEIKRA

Fig. 2.

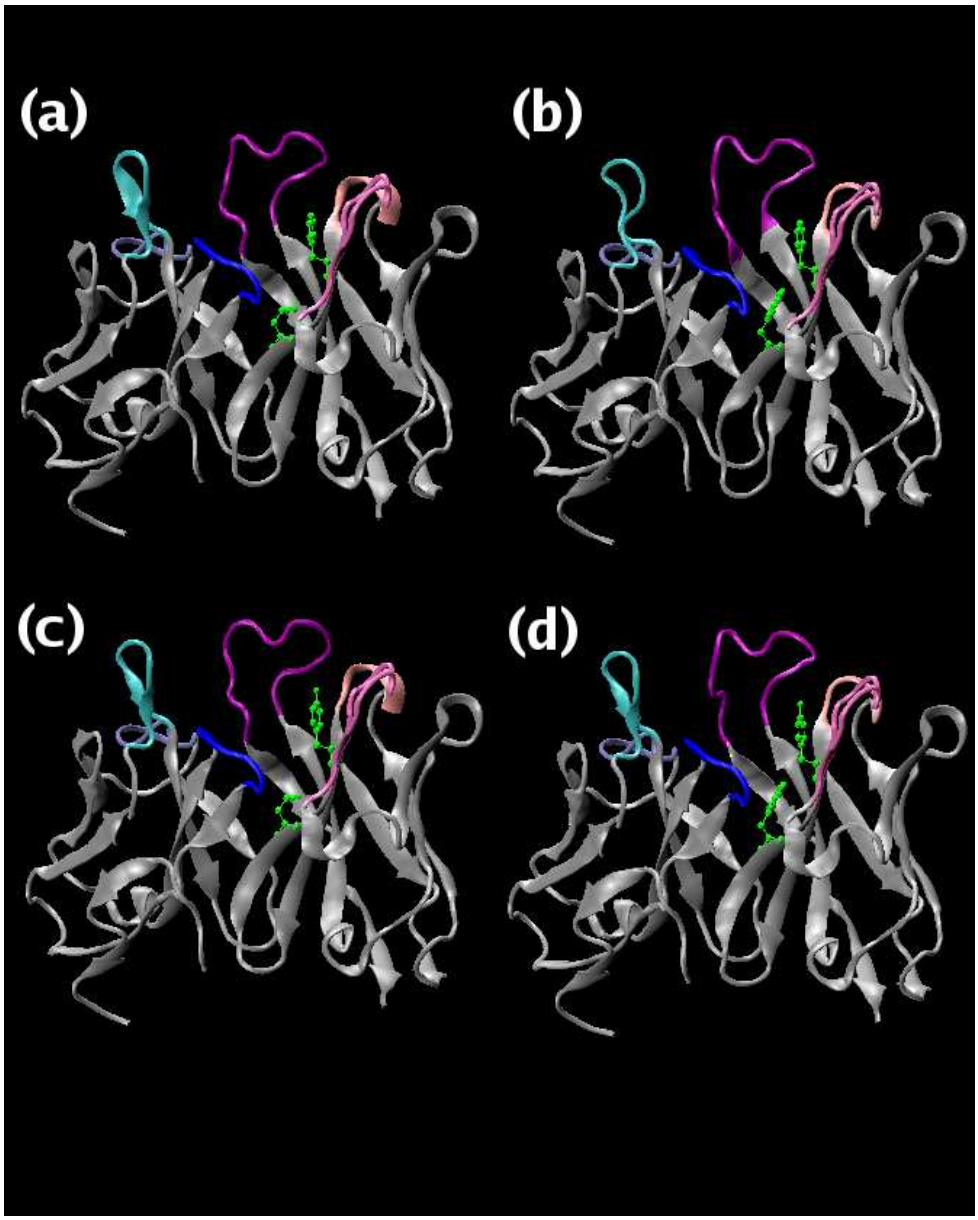

Fig. 3.

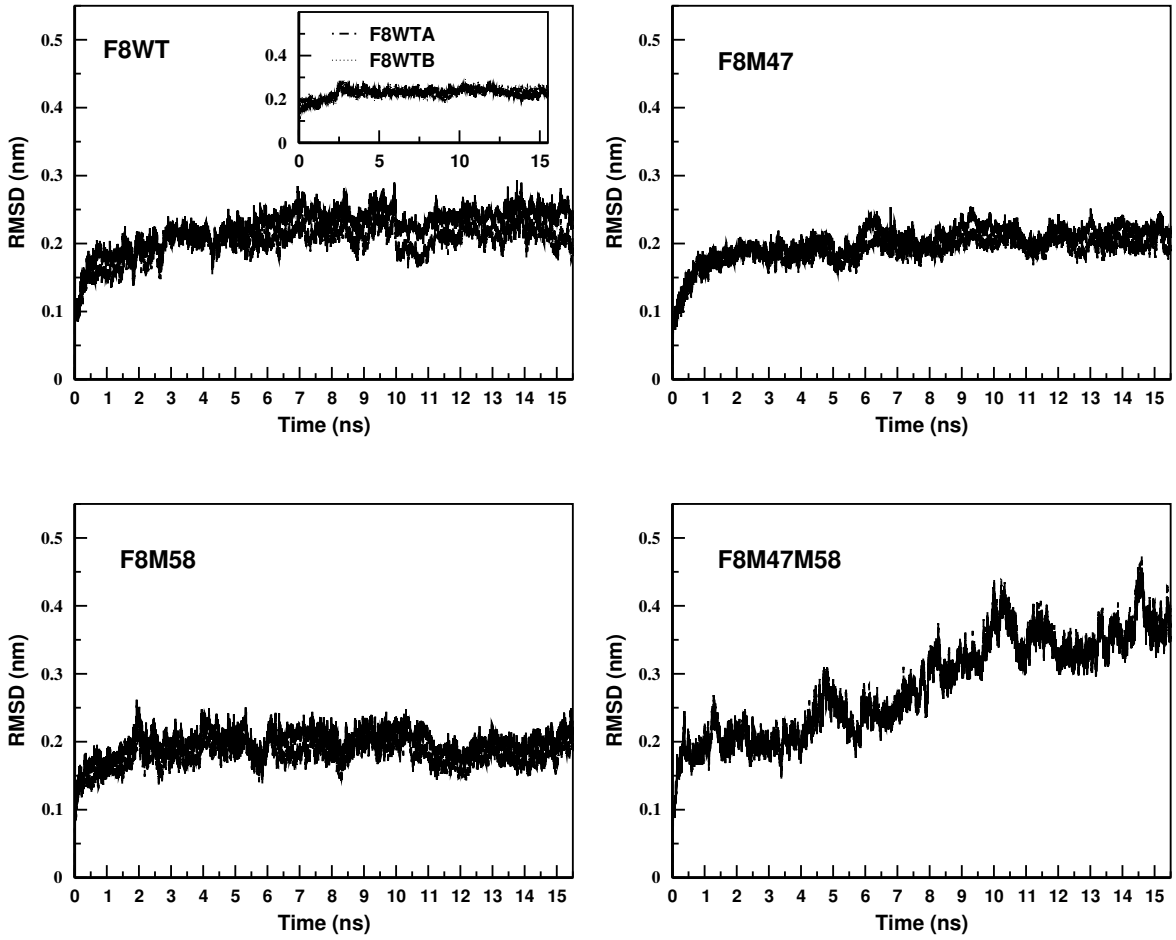

Fig. 4.

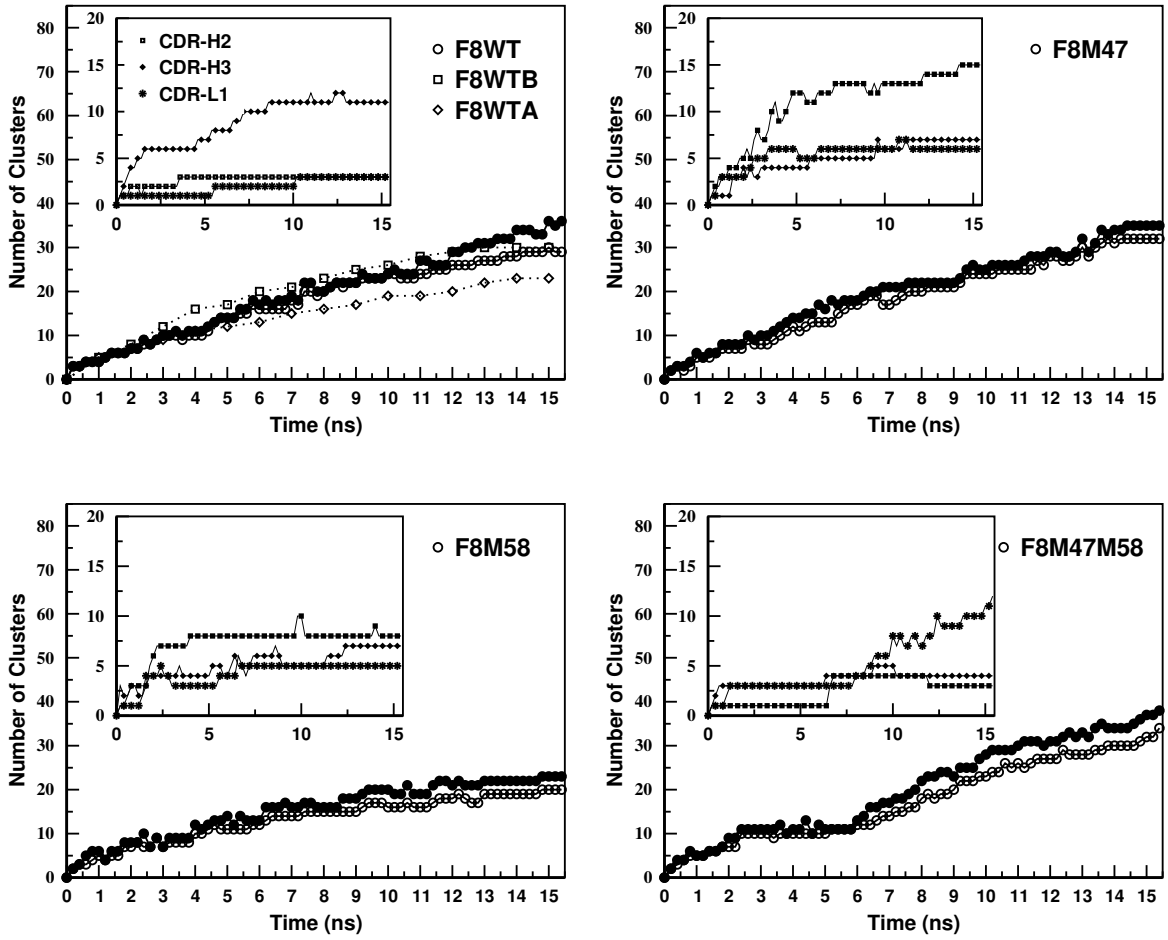
CDR-H2
CDR-H3
CDR-L1
F8WT
F8WTB
F8WTA
F8M47
F8M58
F8M47M58
Number of Clusters
Time (ns)

Fig. 5.

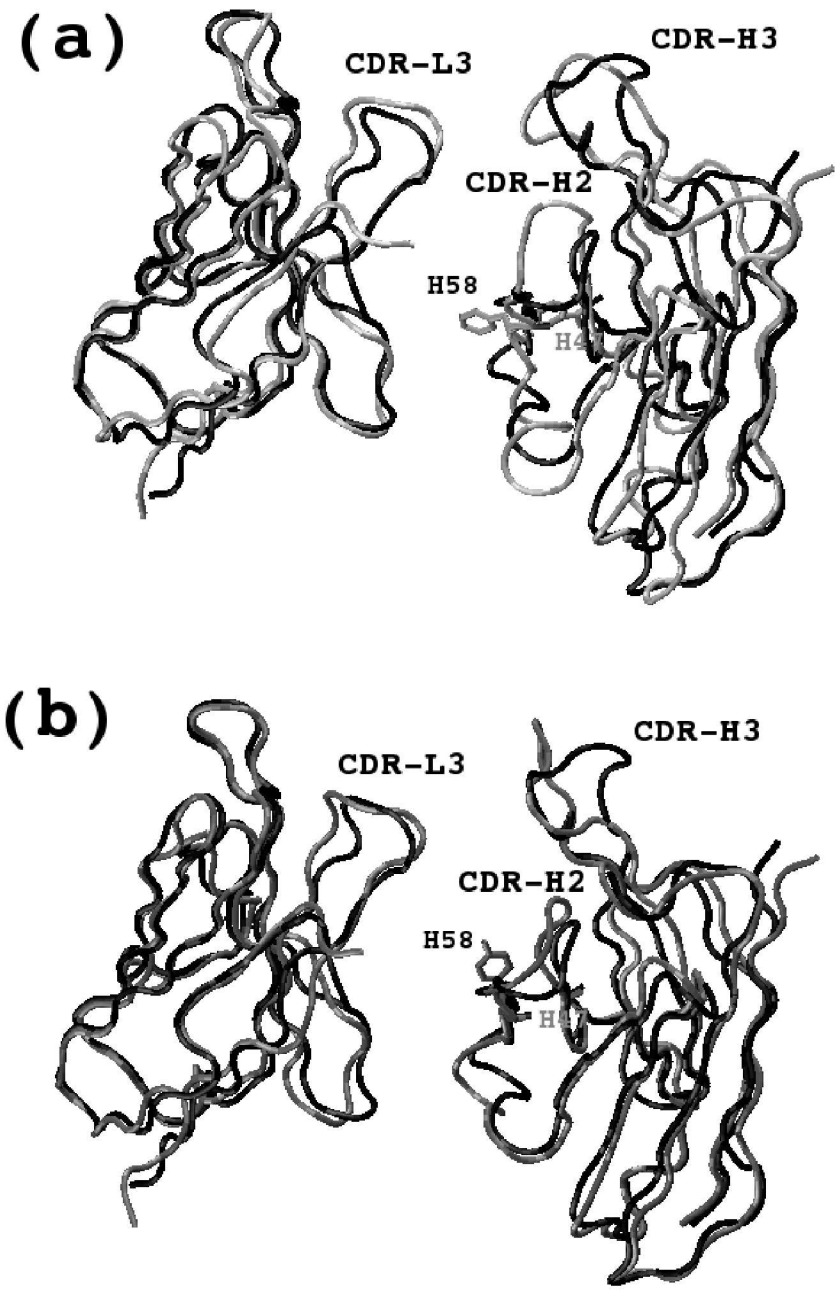

Fig. 6.

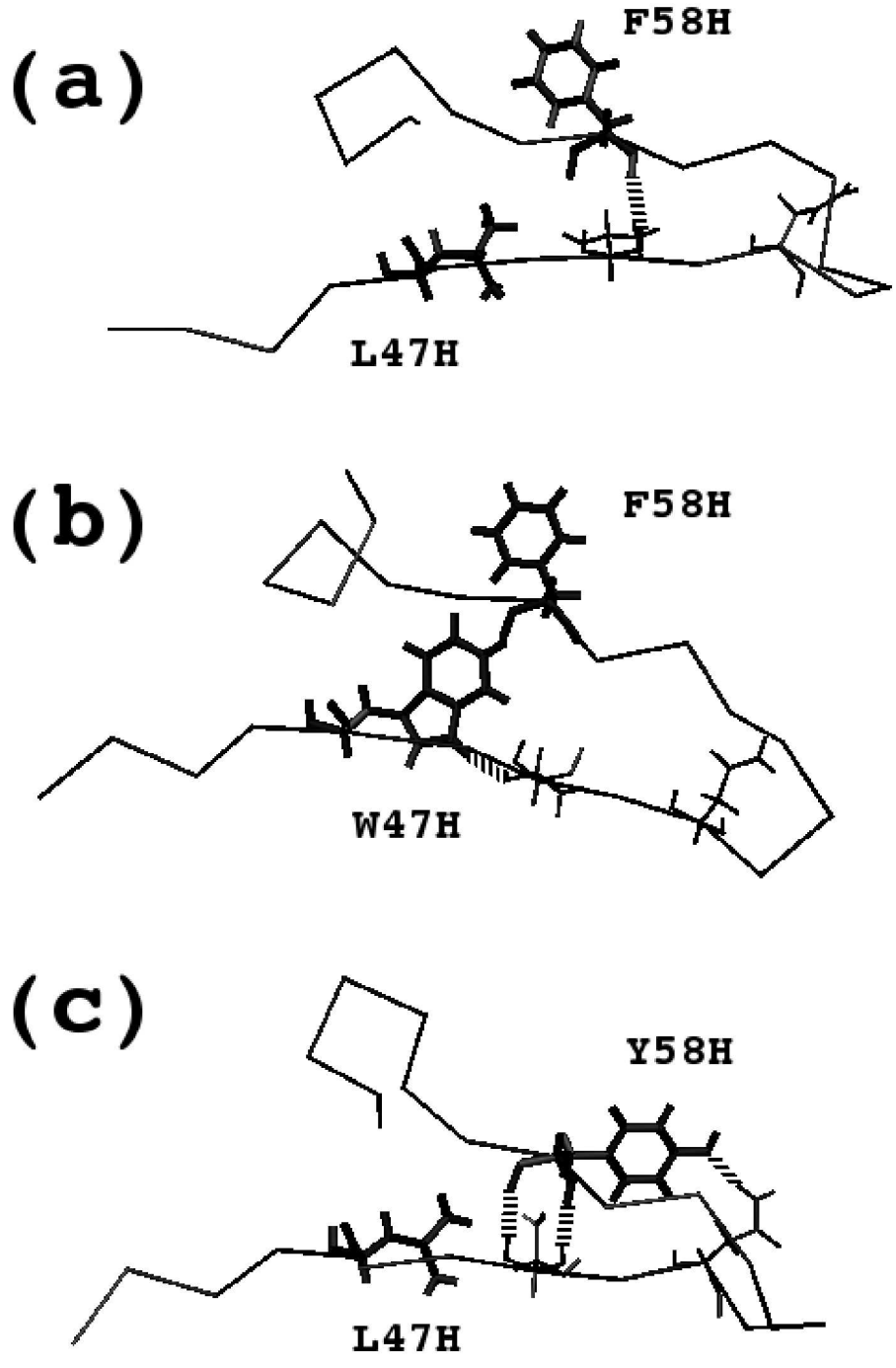

Fig. 7.

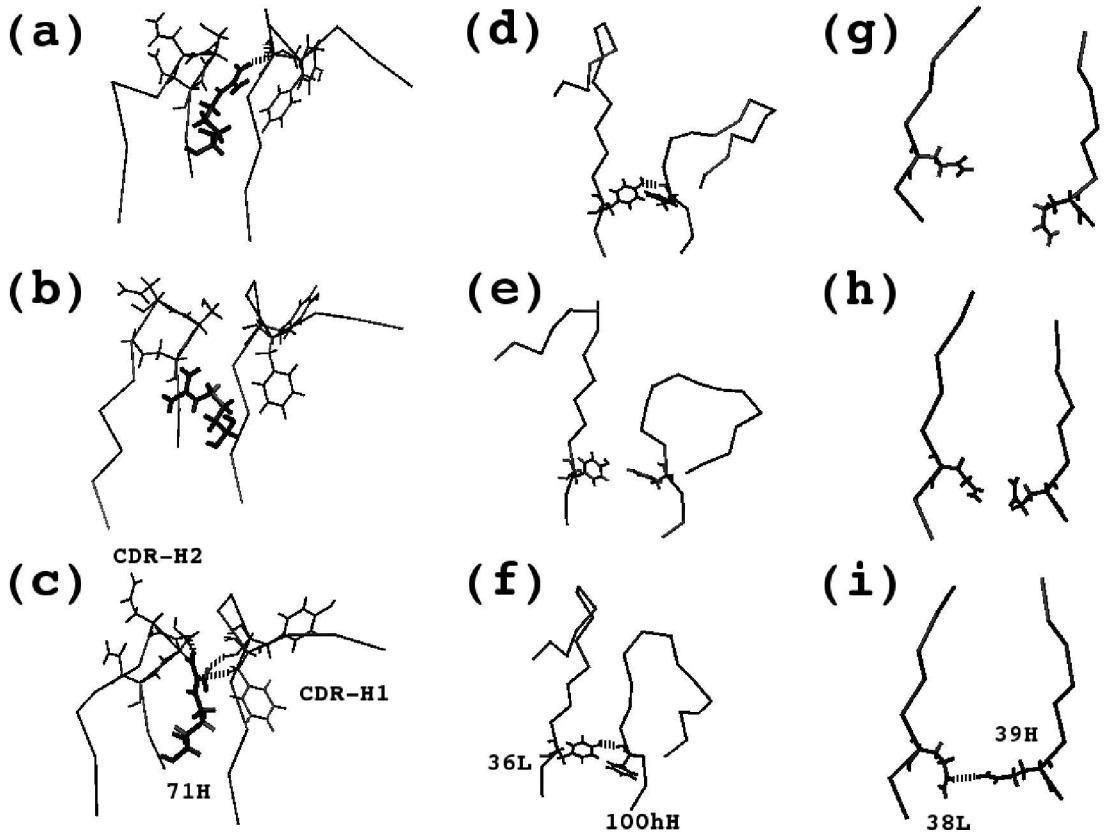

Fig. 8.

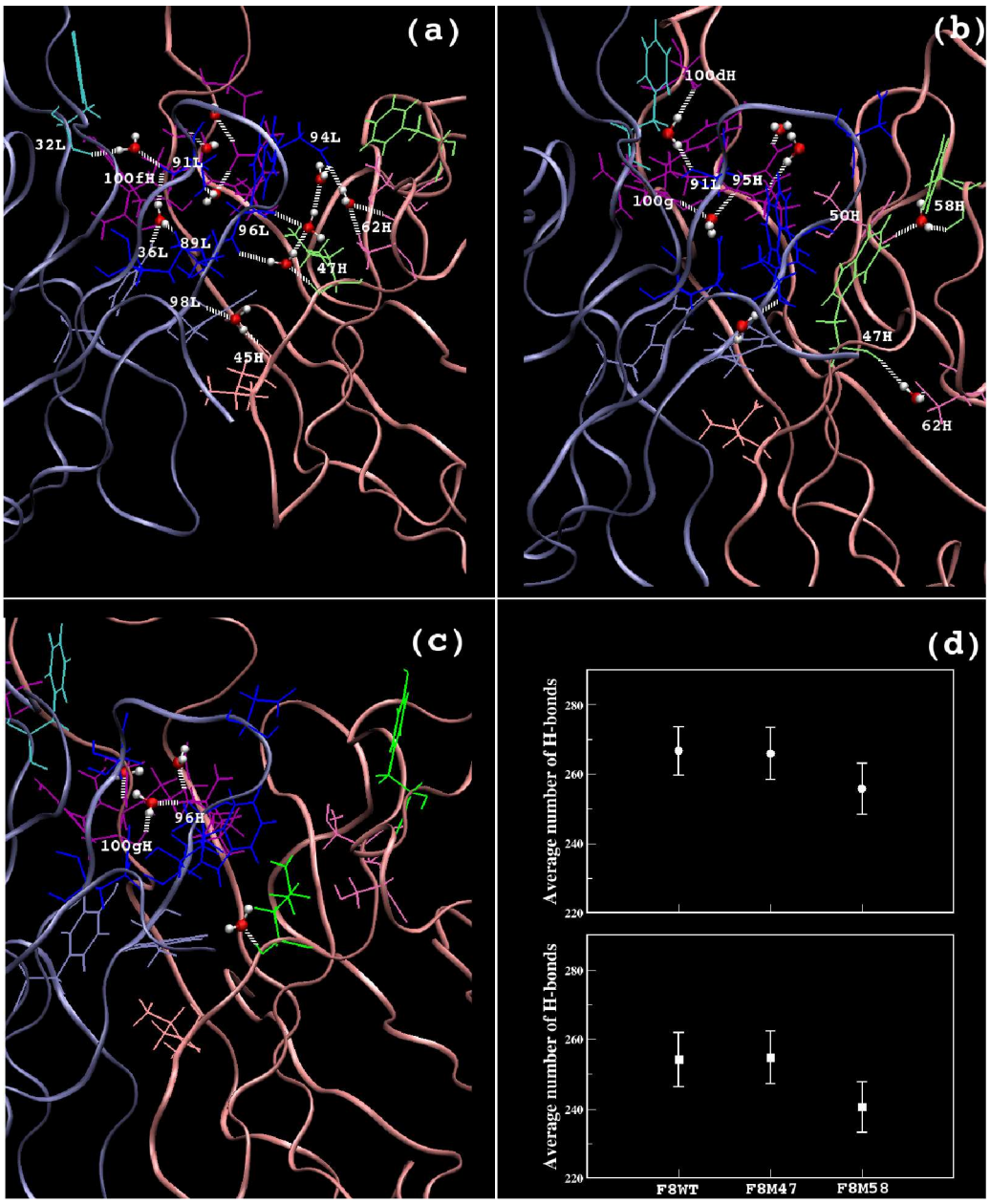
(a)
32L
91L
94L
100fH
96L
62H
36L
89L
47H
98L
45H
(b)
100dH
91L
95H
100g
50H
58H
47H
62H
(c)
96H
100gH
(d)
Average number of H-bonds
280
260
240
220
Average number of H-bonds
280
260
240
220
F8WT
F8M47
F8M58

Fig. 9.

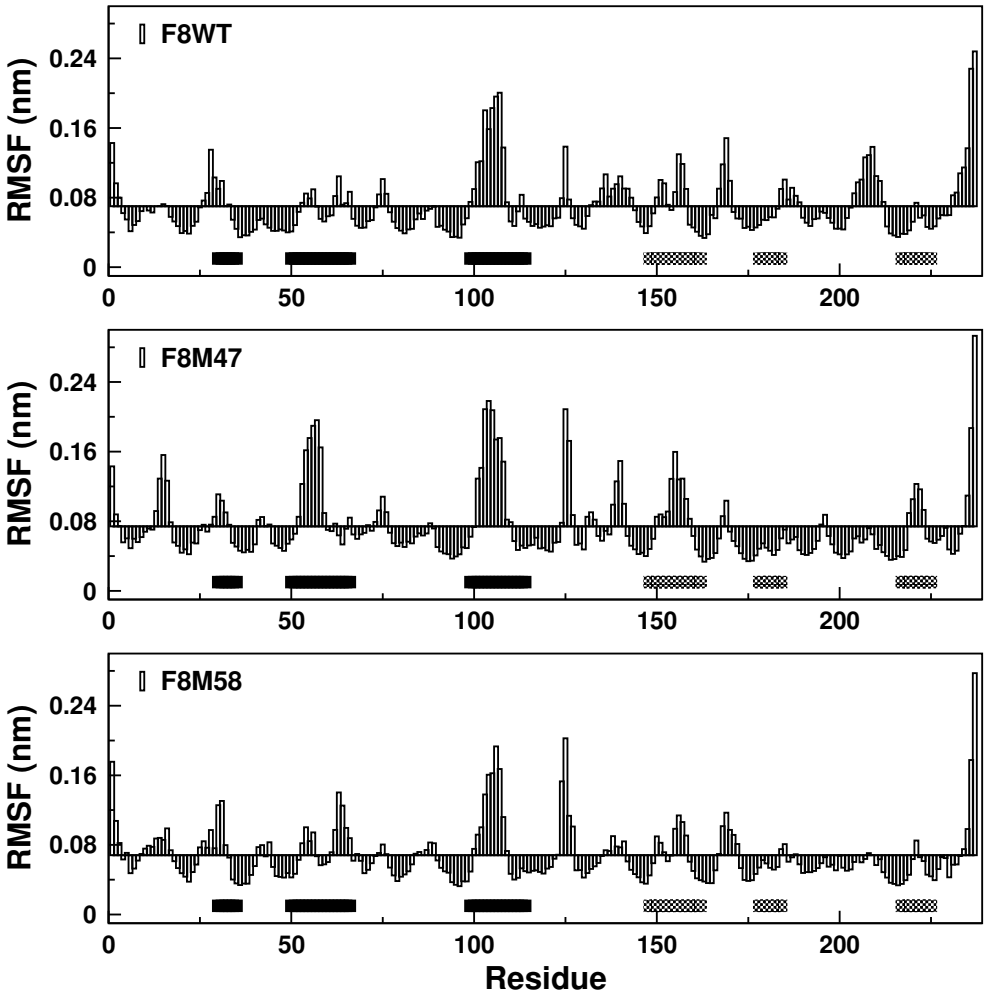

Fig. 10.

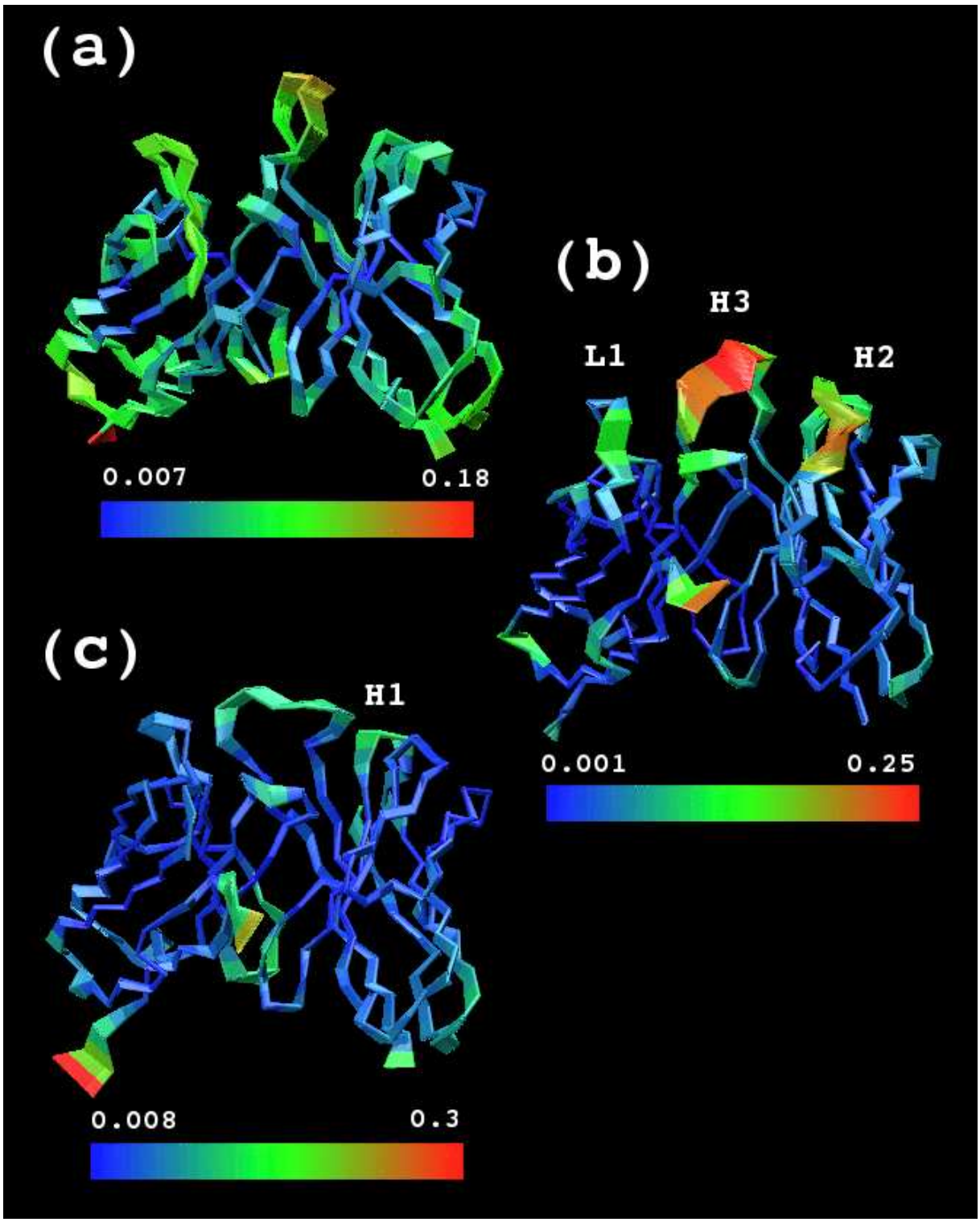

Fig. 11.

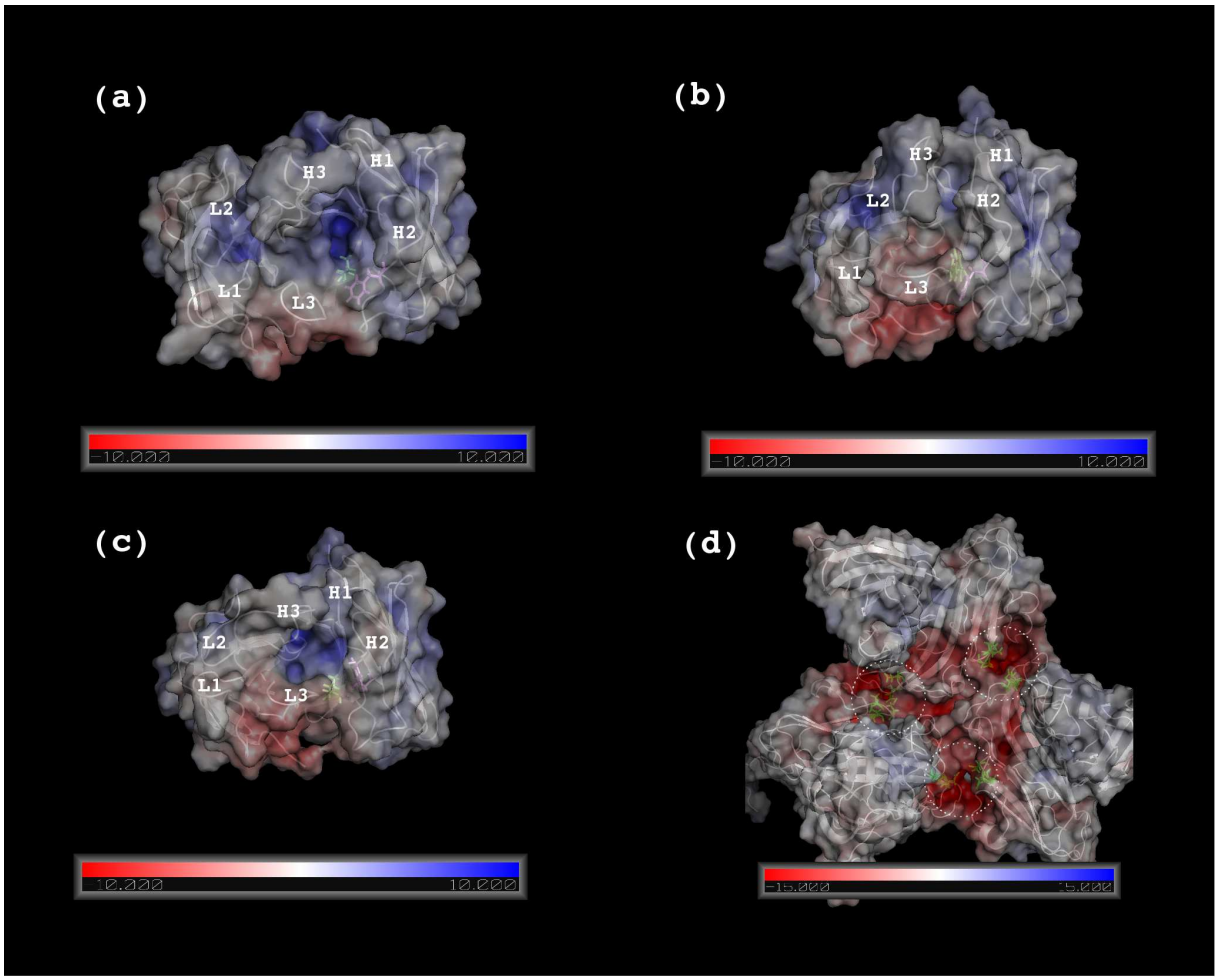
(a)
H3
H1
L2
H2
L1
L3
−10.000
10.000
(b)
H3
H1
L2
H2
L1
L3
−10.000
10.000
(c)
H1
H3
L2
H2
L1
L3
10.000
10.000
(d)
−15.000
5.000

Fig. 12.